Sas3-mediated histone acetylation regulates effector gene activation in a fungal plant pathogen

Running title: Histone acetylation and fungal effector gene regulation

Suarez-Fernandez, Marta[a,b]; Álvarez-Aragón, Rocío[a]; Pastor-Mediavilla, Ana[a]; Maestre-Guillén, Alejandro[a]; del Olmo, Ivan[a]*; De Francesco, Agustina[a]; Meile, Lukas[a]; Sánchez-Vallet, Andrea[a#]

[a] Centro de Biotecnología y Genómica de Plantas (CBGP, UPM-INIA), Universidad Politécnica de Madrid (UPM)—Instituto Nacional de Investigación y Tecnología Agraria y Alimentaria (INIA), Madrid, Spain

[b] Department of Marine Sciences and Applied Biology, Laboratory of Plant Pathology, University of Alicante, Alicante, Spain

Address correspondence to Andrea Sánchez-Vallet, andrea.sanchezv@upm.es

* Current address: Centro de Biología Molecular Severo Ochoa, CSIC-UAM, Madrid, Spain

Keywords: Histone acetylation, *Zymoseptoria tritici*, Sas3, effector gene activation, Gcn5, chromatin remodeling, wheat

Word count of article:

Abstract: 195 words, Importance: 130 words, main text (excluding figure legends, references and materials and methods): 3977 words, Materials and Methods: 1631 words.

ABSTRACT

Effector proteins are secreted by plant pathogens to enable host colonization. Typically, effector genes are tightly regulated, have very low expression levels in axenic conditions, and are strongly induced during host colonization. Chromatin remodeling contributes to the activation of effector genes *in planta* by still poorly known mechanisms. In this work we investigated the role of histone acetylation in effector gene derepression in plant pathogens. We used *Zymoseptoria tritici*, a major pathogen of wheat, as a model to determine the role of lysine acetyltransferases (KATs) in plant infection. We showed that effector gene activation is associated with chromatin remodeling, featuring increased acetylation levels of histone H3 lysine 9 (H3K9) and 14 (H3K14) in effector loci. We functionally characterized the role of *Z. tritici* KATs and demonstrated their distinct contributions to growth, development, and infection. Sas3 is required for host colonization and pycnidia production, while Gcn5 has a major role in pycnidia production. Furthermore, we demonstrated that Sas3 is involved in acetylation of H3K9 and H3K14 in effector loci and in effector gene activation during plant infection. We propose that Sas3-mediated histone acetylation is required for spatiotemporal activation of effector genes and virulence of *Z. tritici*.

IMPORTANCE

Pathogen infections require the production of effectors that enable host colonization. Effectors have diverse functions and are only expressed at certain stages of the infection cycle. Thus, effector genes are tightly regulated by several mechanisms, including chromatin remodeling. Here, we investigate the role of histone acetylation in effector gene activation in the fungal wheat pathogen *Zymoseptoria tritici*. We demonstrated that lysine acetyltransferases (KATs) are essential for the spatiotemporal regulation of effector genes. We show that two KATs, Sas3 and Gcn5, are involved in leaf symptom development and pycnidia formation. Importantly, our results indicated that Sas3 controls histone acetylation of effector loci and is a regulator of effector gene activation during stomatal penetration. Overall, our work demonstrates the key role of histone acetylation in regulating gene expression associated with plant infection.

1. INTRODUCTION

Plant pathogens produce and secrete effectors into host tissues to facilitate colonization. Effectors have several functions including suppression of the immune response, alteration of plant development, acquisition of nutrients, and interference with the host microbiota (1). Effectors are frequently required at specific phases of the infection cycle (2). Consequently, the transcriptional control of effector genes is key to provide the pathogen with a dynamic infection machinery. Despite the importance of tight effector gene regulation in fungal plant pathogens, the mechanisms involved remain mostly enigmatic.

Chromatin remodeling is a pivotal mechanism of gene regulation and involves post-translational modifications of histone tails, such as acetylation and methylation. These modifications provide a conserved mechanism that modulates the accessibility of the transcription machinery to the DNA and thereby alters gene expression (3–5). Writing enzymes, including methylases, acetylases and erasing enzymes, such as demethylases and deacetylases, are dynamically involved in the posttranscriptional modification of histone tails in eukaryotes (6, 7). Effector genes are frequently located in heterochromatic regions of the genome (8, 9). In plant-associated fungi, including *Leptosphaeria maculans*, *Epichloë festucae*, *Magnaporthe oryzae* and *Zymoseptoria tritici*, effector genes are enriched in trimethylation of histone H3 lysine 9 (H3K9) and/or 27 (H3K27) in the absence of the host (10–13). During plant colonization, effector gene activation is associated with a tightly regulated reduction in the methylation levels in H3K9 and/or H3K27, as shown in *E. festucae* and *Z. tritici*. Accordingly, disruption of the key enzymes involved in methylation of H3K27 or H3K9 has been shown to enhance expression of effector genes and secondary metabolite gene clusters (10, 13). Thus, derepression of effector genes during host colonization involves changes in the chromatin state.

Although acetylation of specific residues of core histone tails has been shown to regulate transcription in eukaryotes (6, 7), the role of lysine acetyltransferases (KATs) in the overall fitness of fungal pathogens and in the spatiotemporal expression activation of effector genes remains to be largely understood. KATs transfer acetyl groups from acetyl-coenzyme A onto lysine residues of core histones and commonly form part of complexes (7). Frequently, KAT complexes harbor regulatory components that regulate KAT activity and substrate specificity to prevent uncontrolled histone acetylation (14). KATs are classified into different families, including the GNAT (from Gcn5-related N-acetyltransferase) and the MYST (MOZ, YBF2/SAS3, SAS2, and TIP60) families (7). Histone acetylation in filamentous fungi has been reported to regulate several biological processes such as growth, reproduction, secondary metabolite synthesis and

pathogenicity. For instance, orthologues of Gcn5 mediate dimorphic changes, tolerance to stress, and virulence in *Ustilago maydis* (15), secondary metabolite regulation in *Aspergillus nidulans* (16), and stress tolerance and conidiation in *Alternaria alternata* (17). KATs from the MYST family are involved in growth and conidiation of *M. oryzae* and *A. alternata* (17, 18). In *Fusarium graminearum* KATs from the GNAT and MYST families mediate secondary metabolite regulation and virulence (19), highlighting the complexity of the role of KATs in trait regulation in fungi. Remarkably, histone acetylation is not only involved in fungus-plant interactions but also in fungus-bacterium interactions. Upon interaction of the filamentous fungus *A. nidulans* with the bacterium *Streptomyces rapamycinicus,* fungal secondary metabolite gene clusters are induced. This process involves acetylation of H3K9 and acetylation of histone H3 at lysine 14 (H3K14), and Gcn5 protein activity (16). Likewise, we hypothesized that histone acetylation plays a major role in effector gene activation in fungus-plant interactions. Given the important role of KATs in transcriptional activation in Eukaryotes and given the fact that effector genes are derepressed during host colonization (15–18), we propose that an increase of histone acetylation levels regulates activation of pathogen effector genes during plant infection.

Z. tritici is a major pathogen of wheat, causing significant yield losses in temperate climates (20). The infection cycle of *Z. tritici* initiates at the leaf surface with the germination of asexual or sexual spores. Emerged hyphae grow on the leaf surface and penetrate through the stomata. Subsequently, *Z. tritici* colonizes the apoplast and, after several days of infection, forms asexual fruiting bodies known as pycnidia (21). Chlorotic and necrotic symptoms are only observed after several days of infection of the pathogen, prior to asexual reproduction (22). *Z. tritici* mainly grows as a filamentous fungus on wheat leaf surfaces but can also grow as blastospores *in vitro* on rich media and occasionally on the leaf surface (23). Various effector genes are strongly induced during plant infection at different stages of the *Z. tritici* life cycle, *AvrStb6* and *Avr3D1* being activated during stomatal penetration and apoplast colonization, while *Mycgr3G76589* is expressed at later stages of the infection life cycle (10, 24, 25). Promoter activity and local reduction of histone methylation levels are required for the specific expression pattern of effector genes (10). Our integrative study aimed to determine the role of histone acetylation and KATs in effector gene regulation in *Z. tritici*. We demonstrated that dynamic histone acetylation of H3K9 and H3K14 is associated with expression activation of effector genes and host colonization.

2. RESULTS

2.1 *Z. tritici* has 7 orthologues of KATs

We first aimed to identify KAT orthologues in *Z. tritici*. To achieve this, we performed a BLAST search on annotated *Z. tritici* genes using previously characterized *Saccharomyces cerevisiae* KATs as queries. In addition, we used the dbHiMo database (26), which comprises histone-modifying enzymes from several fungal species including *Z. tritici*. A reverse BLAST analysis with the identified putative *Z. tritici* KAT orthologues was subsequently performed on the *S. cerevisiae* genome. We found 3 KAT orthologues from the MYST family, 2 from the GNAT family, and 1 from the specific fungal family RTT109 (Table 1). Additionally, 1 orthologue of Gcn5-related N-acetyltransferase (Ngs1; Table 1) previously identified in *Candida albicans* was also identified in *Z. tritici* (27).

The BLASTp (Table S1) and dbHiMo analyses provided a consistent classification of 3D7.g7031 as Sas2 (KAT8) and 3D7.g9281 as Esa1 (KAT5). However, the classification of 3D7.g4263 was conflicting since dbHiMo predicted it to be Esa1, while the BLASTp analysis classified it as a Sas3 protein. To properly classify KAT orthologues, a phylogenetic tree was constructed using KATs of the MYST family from different fungal species. The phylogenetic analysis showed that 3D7.g4263 clusters with Sas3 (KAT6) protein orthologues, that 3D7.g7031 is a Sas2 orthologue, and that 3D7.g9281 is an Esa1 orthologue (Figure 1A; Table S2; Table 1). We identified the expected MOZ/SAS domain and the MYST family zinc finger domain in the *Z. tritici* orthologues of Esa1 and Sas2 using HMMER (Figure 1C). In addition to these two domains, Esa1 harbors an RNA-binding domain near the N-terminus. Sas3 is the largest protein identified and contains two MOZ/SAS domains next to a MYST family zinc finger domain and a plant homeodomain (PHD) -finger domain.

The phylogenetic analysis of KATs of the GNAT family indicated that 3D7.g2851, 3D7.g4775 and 3D7.g8500 cluster with Ngs1, Gcn5 (KAT2) and Elp3 (KAT9) proteins, respectively (Figure 1B; Table S2; Table 1). All the identified KAT orthologues belonging to the GNAT family contain a GNAT acetyltransferase domain. Gcn5 additionally has a bromodomain in its C-terminal region, while the Elp3 orthologue contains 2 radical SAM domains. Ngs1 contains a glycosyl hydrolase family 3 (GH3) domain (Figure 1C), as previously described for orthologues of this KAT in other organisms (27).

2.2 KAT genes in *Z. tritici* are differentially expressed during plant infection

We hypothesized that KATs involved in effector gene regulation might be expressed during plant infection and they might exhibit a similar expression pattern as effector genes. Therefore, we performed a transcriptomic analysis of the genes encoding the identified KATs and compared them with the expression of three effector genes formerly shown to be epigenetically regulated (10): *Avr3D1* (24), *AvrStb6* (25) and *Mycgr3G76589* (28). For this purpose, we used data from previously published RNA-seq studies (23, 29). The MYST family orthologues (*Esa1*, *Sas2* and *Sas3*) were expressed during host colonization, displaying low expression levels at the beginning of the infection and a peak of expression at 12-14 days post-infection (dpi). The three GNAT family members were also expressed during host colonization, *Elp3* exhibiting the lowest expression levels at 14 dpi (Figure 2). Based on the different gene expression patterns of the KAT members, we hypothesized that they might have distinct roles in growth, development, and virulence.

2.3 Histone acetylation levels in effector loci increase during plant infection

To evaluate the changes in acetylation of H3K9 and H3K14 during plant infection in effector loci, we performed a chromatin immunoprecipitation assay followed by quantitative PCR (ChIP-qPCR). We infected wheat plants with *Z. tritici* and harvested the second leave at 11 dpi, which is approximately the time point at which maximum levels of effector transcripts can be observed (Figure 2; (10)). We additionally analyzed histone acetylation in *Z. tritici* grown under axenic conditions. We evaluated the acetylation levels of H3K9 and H3K14 in different regions of *AvrStb6*: 1000 base pairs (bp; -1000), 500 bp (-500), 300 bp (-300) and 50 bp (-50) upstream of the start codon, and within the open reading frame region (ORF). We also evaluated the acetylation of these two marks 300 bp upstream of the start codon of *Avr3D1*. A TFIIIC transcription factor complex unit (*3D7.g8520*; *TFIIIC*) was used as control. As expected (30, 31), the acetylation levels of the control and *AvrStb6* (-1000) remained stable *in planta* compared to axenic conditions. We observed an increase in the acetylation levels of H3K9 and H3K14 at the loci of the effector genes *Avr3D1* and *AvrStb6* (Figure 3). The ChIP-qPCR results support a possible role of histone acetylation in the activation of effector genes during infection.

2.4 KAT orthologues in *Z. tritici* are involved in growth and colony development

To determine the function of the KAT orthologues of *Z. tritici* in development and virulence, we obtained loss-of-function mutants in the genes *Sas2*, *Sas3*, *Ngs1*, *Gcn5* and *Elp3*. We first determined the role of the investigated KATs in development. We measured the area of colonies of the KAT mutants grown on yeast-malt-sucrose agar (YMA; Figure S1). Δ*Sas3* and Δ*Gcn5*

colonies were significantly smaller than colonies of the control. Interestingly, Δ*Sas2* lines displayed the opposite phenotype, with larger colony diameters than the controls, most likely due to their hyphal-like growth, as observed on the colony edges (Figure S1). We therefore suggest that Sas2, Sas3 and Gcn5 might be involved in growth and/or development, with Sas2 probably being a negative regulator of growth and hyphal switch.

We addressed the role of the KATs in stress tolerance by assessing the performance of the mutants under different stresses, including high temperature (28°C), salt (NaCl; 0.5 M), H_2O_2 (1 mM), osmotic (sorbitol; 1 M) and cell wall (Calcofluor white; 200 ng·µL^{-1}, and Congo red; 2 mg·mL^{-1}) stresses on YMA. Additionally, we quantified growth in the presence of different carbon sources, such as fructose (5 g·L^{-1}), galactose (50 mM), N-acetylglucosamine (GlcNAc, 2.5 mM), and glucose (2.5 mM) in a nutrient poor minimal medium (MM). Colony development of the mutants was compared with growth under standard conditions (YMA 18°C) and to the control line (3D7-GFP). Δ*Sas3* colonies were smaller than those of the control line under all the conditions, supporting the role of Sas3 in growth and/or development. The other tested mutants grew similarly to 3D7-GFP under all the stress conditions, except for Δ*Gcn5* and Δ*Ngs1*, which were slightly more resistant to Congo red than the control line (Figure S2). Therefore, we concluded that *Z. tritici* KATs are not positive regulators of stress tolerance.

2.5 Sas3 and Gcn5 are involved in virulence

We further investigated the role of KATs in host colonization on the susceptible wheat cultivar Runal (Figure 4; Figures S3 and S4). All the KAT mutants developed a similar biomass to that of the control at 10 dpi, except for Δ*Sas3* and Δ*Ngs1*, which had a significantly lower biomass (Figure 4A). However, at shorter time points (6 dpi), Δ*Sas3* grew to similar levels as the control (Figure 4B; Figure S5). In accordance with the reduction in biomass, Δ*Sas3* developed less disease symptoms, as determined by the percentage of leaf area covered by lesions (PLACL), and less pycnidia (Figure 4; Figures S3 and S6). Additionally, we observed a slightly faster production of symptoms by the mutant Δ*Gcn5* (Figure 4D; Figures S4 and S6). Nevertheless, this faster spread of disease symptoms did not lead to a higher production of pycnidia. Instead, we observed that Δ*Gcn5* generated very few pycnidia (Figure 4E; Figures S4, S6 and S7). Δ*Elp3* showed a slight reduction in pycnidia production per leaf lesion at 20 dpi (Figure 4E; Figure S4), suggesting a contribution of Elp3 to asexual reproduction. Additionally, Δ*Sas2* showed a slightly altered infection phenotype, manifested by red/orange spots on infected leaves, but no differences in PLACL or in pycnidia production were detected (Figure 4; Figures S3 and S6). Overall, *Gcn5* and *Sas3* disruption led to the highest effect on virulence and/or pycnidia

production. To confirm that the observed phenotype of Δ*Gcn5* and Δ*Sas3* was due to the disruption of the KAT genes, we obtained complementation lines which expressed the wildtype version of *Gcn5* and *Sas3* in the mutant backgrounds. We observed a restoration of virulence and pycnidia production in both complementation lines (Figure S7). These results demonstrate that Sas3 is involved in virulence and that Sas3 and Gcn5 mediate pycnidia formation, indicating the key role of *Z. tritici* KATs in virulence and reproduction.

2.6 KAT mutants are impaired in expression regulation of effector genes under axenic conditions

We next determined the role of *Z. tritici* KATs in regulation of the infection machinery by analyzing the expression levels of the effector genes *Avr3D1*, *AvrStb6* and *Mycgr3G76589* by qRT-PCR under axenic conditions. The expression of *Avr3D1* was drastically reduced in Δ*Sas3* (Figure 5A), and the expression of *AvrStb6* was reduced in Δ*Sas2,* Δ*Sas3* and Δ*Gcn5* (Figure 5B) under axenic conditions. *Mycgr3G76589* expression was unchanged in the mutants (Figure S8).

To determine the role of the investigated KATs in effector gene regulation at the cellular level, we disrupted the KAT genes in a reporter line that harbors His1-mCherry located at the *AvrStb6* locus, and under the control of the *AvrStb6* promoter (10). The fusion of histone 1 (His1) with mCherry enabled its nuclear localization and allowed monitoring *AvrStb6* expression at the cellular level. In the control reporter line growing under axenic conditions, mCherry was detected, indicating that the *AvrStb6* promoter is partially active when *Z. tritici* grows in the absence of the host (Figures 5C and 2). Δ*Ngs1* and Δ*Elp3* showed the same expression pattern as the control (Figures 5F and 5H), while Δ*Sas2*, Δ*Sas3* and Δ*Gcn5* showed a decrease in the levels of mCherry accumulation under axenic conditions (Figures 5D, 5E and 5G). These results confirmed that *Z. tritici* Sas2, Sas3 and Gcn5 are involved in effector gene regulation under axenic conditions.

2.7 Effector gene expression is altered during plant infection in the KAT mutants

Effector genes are key for plant colonization and highly induced during infection (Figure 2). We hypothesized that histone acetylation might be required for effector gene upregulation. We determined the expression levels of 4 effector genes (*Avr3D1* (*3D7.g7883* reannotated in (24)), *AvrStb6* (*3D7.g5586*), *AvrStb9* (*3D7.g741*; (32)), and *Mycgr3G76589* (*3D7.g10118*)) by qRT-PCR during plant infection in KAT knockouts (Figure 6). The expression levels of *Avr3D1* and *AvrStb6* were higher in Δ*Ngs1* and Δ*Gcn5*, while *AvrStb6* expression was reduced in Δ*Sas2* and Δ*Sas3* at 10 dpi (Figures 6A and 6B). We also observed reduced expression of *Mycgr3G76589* in all mutants except Δ*Gcn5* (Figure 6D) and a reduction of *AvrStb9* expression in Δ*Sas3* (Figure 6C).

These results suggest that KATs are involved in infection and in the proper regulation of effector gene expression during early stages of plant colonization.

The above qRT-PCR analyses do not resolve expression levels in individual cells. The reporter line harboring the mCherry gene expressed under the control of the *AvrStb6* promoter and located in the *AvrStb6* locus enabled us to monitor the *AvrStb6* expression pattern at the cellular level. Confocal microscopy pictures were taken at 6 dpi to maximize the number of penetration events of *Z. tritici*, while minimizing the autofluorescence produced by plants at later time points of the infection. The *AvrStb6* promoter shows little activity during hyphal growth on the plant surface but is strongly activated in hyphae approaching the stomata (Figure 6D), as previously demonstrated (10). We investigated whether this expression pattern was mediated by KATs. Remarkably, all the analyzed mutants grew as hyphae on the leaf surface and reached leaf stomata. Interestingly, at 6 dpi, Δ*Sas3* showed only minimal activation of the *AvrStb6* promoter even in hyphae attempting to penetrate the stomata (Figure 6F), which confirms the previous observation of Sas3 being involved in effector gene regulation during infection. On the other hand, the activity of the *AvrStb6* promoter in Δ*Elp3* was higher than in the control regardless of the proximity to stomata (Figure 6I). Δ*Sas2*, Δ*Ngs1* and Δ*Gcn5* displayed a similar *AvrStb6* expression pattern than the control at 6 dpi (Figures 6E, 6G and 6H). The results demonstrate that Sas3 is involved in effector gene upregulation during stomata penetration in *Z. tritici*.

2.8 Sas3 contributes to H3K9 and H3K14 acetylation of effector loci during plant infection

We subsequently evaluated whether Sas3-mediated expression regulation of effector genes is associated with histone acetylation during plant infection. We determined the acetylation levels of H3K9 and H3K14 during wheat infection in Δ*Sas3* lines. We observed a reduction in the relative acetylation levels of H3K9 (Figure 7A) and H3K14 (Figure 7B) in the *AvrStb6* promoter region and in *Avr3D1* in Δ*Sas3* compared to the control line during plant infection. As expected, acetylation levels of H3K9 and H3K14 in the control locus (*TFIIIC*) and 1000 bp upstream of the start codon of *AvrStb6* were not affected by the *Sas3* deletion. These results demonstrate that Sas3 is involved in plant-associated acetylation of H3K9 and H3K14 in effector loci. We suggest that the reduced effector transcript levels and the hindered infection of Δ*Sas3* (Figures 4 and 6) might be due to a reduction in histone acetylation (Figure 7).

3. DISCUSSION

Exploring the mechanisms by which plant pathogens activate their infection machinery is key for understanding how the interaction between the host and the pathogen is established. In the past years, chromatin remodeling has been shown to be crucial for effector gene activation during plant infection (10, 11, 13, 33). However, the specific chromatin modifications that are involved in this activation remain largely unknown. In this work we investigated the role of KATs and histone acetylation in the virulence of the fungal plant pathogen *Z. tritici.* We demonstrated that Sas3-mediated histone acetylation dynamics are associated with upregulation of effector genes during plant infection.

A total of three KATs from the MYST family were identified in *Z. tritici*, Sas3, Sas2 and Esa1. We showed that Sas3 and Sas2 are involved in the expression regulation of well-characterized effector genes, such as *AvrStb6*. Although Sas2 did not affect asexual reproduction and the speed at which necrotic lesions developed, it clearly shaped the visual appearance of lesions, manifested by red-orange spots in lesions produced in infections by the *ΔSas2* mutant. We considered that this altered symptom development might be the result of misexpression of *AvrStb6* and potentially other effector genes in the *ΔSas2* mutant. Likewise, the Sas2 orthologue in *B. cinerea* (BcSas2) is involved in regulation of virulence (34), suggesting a conserved role of Sas2 in effector gene activation in fungal pathogens. Disruption of *Sas3* in *Z. tritici* led to a reduction of virulence and pycnidia formation. Similarly, Sas3 from *M. oryzae* is involved in virulence (18). We additionally noticed that Sas3 is required for normal growth under axenic conditions since colony size was reduced in *ΔSas3*. Although this reduction in growth could indirectly lead to a reduction of virulence, we suggest that Sas3 is directly involved in the regulation of virulence since (i) *ΔSas3* grows as hyphae on the leaf surface of wheat and are able to reach the stomata, (ii) *AvrStb6* activation is impaired in the proximity to the stomata in *ΔSas3* mutants, and (iii) misactivation of effector genes occurs at stages of infection when the fungal biomass is similar to the control (6 dpi). Thus, we believe that the impaired virulence of *ΔSas3* mutants is most likely a consequence of effector gene misregulation, featuring reduced expression levels of *AvrStb6*, *AvrStb9,* and *Mycgr3G76589* during plant infection, highlighting the contribution of Sas3 in the activation of effector genes. (30). Remarkably, mutants in Sas3 are impaired in histone acetylation of effector genes during plant infection, suggesting that Sas3-mediated acetylation is a crucial mechanism driving the transcriptional reprogramming of effector genes during plant infection *Z. tritici* (16).

We identified three members of the GNAT KAT family in *Z. tritici*, with distinct roles in the infection cycle. Expression analysis of effector genes in GNAT mutants revealed that GNATs

might be involved in negatively regulating effector genes. However, GNATs might not directly regulate effector genes but rather other transcriptional regulators. We suggest that in Δ*Gcn5* the higher expression levels of effector genes might lead to faster development of necrosis. This might be due to two possible scenarios. The high accumulation of effectors might lead to an early recognition of the pathogen by the host, resulting in a strong immune response which might be manifested by cell death. Alternatively, misregulation of cell-death inducing effectors might directly produce necrosis at earlier stages of the infection. Additionally, we showed that Gcn5 is involved in asexual reproduction since the knockout mutant developed relatively few pycnidia. Interestingly, Gcn5 negatively regulates symptom development but positively regulates reproduction, supporting that different mechanisms govern virulence and pycnidia production, as previously shown (23).

H3K9 and H3K14 acetylation are well-known euchromatic marks (35). Accordingly, we observed an increase in histone acetylation levels in *Avr3D1* and *AvrStb6* during plant infection, along with the derepression of these two effector genes. We suggest that this increase in histone acetylation levels contributes to the *in planta*-specific upregulation of effector genes in *Z. tritici*. Previously, we reported a decrease in the levels of H3K27 and H3K9 trimethylation in effector loci during plant infection associated with effector gene depression (10). We consider that this reduction of histone repressive marks and an increase in activating marks, such as those described in the current work, promote a local switch from repressive to permissive chromatin, allowing the access of nucleosome remodeling complexes and structural modifications in chromatin, including decondensation of the chromatin fiber. Previous work demonstrated that for selected effector genes, such changes in chromatin structure are very local and do not affect neighboring loci (10), suggesting the targeted location of KATs to effector loci during plant infection. Substrate specificities have been reported to be mediated by certain subunits from KAT complexes or KAT domains that interact with nucleosomes (36). In *Z. tritici*, a bromodomain and a PHD-finger domain were identified in Gcn5 and Sas3, respectively, both with a potential role in substrate specificity or in interaction with regulatory proteins (37). In addition, the concerted expression of effector genes during plant infection most likely requires altered transcription factor activities or levels, as demonstrated for the Zn2Cys6 family member transcription factor Pf2 from *L. maculans*. In this case, the coordinated action of trimethylation of H3K9 and Pf2 governs the specific expression pattern of effector genes (38). Accordingly, we propose that chromatin modifications and still unknown transcription factors might jointly act as derepressors of effector genes of *Z. tritici* during plant infection.

We have shown that histone modifications, involving acetylation and demethylation (10), mediate the activation of effector genes during plant infection. Elucidating the crosstalk between histone modifications, their direct or indirect function in effector gene regulation and the role of classic transcriptional activators and repressors will help us to further understand the molecular mechanisms linking chromatin and stage-specific transcriptional changes. Future work aiming to unveil global changes in histone acetylation and methylation patterns during plant infection will shed more light on the contribution of these histone marks to the regulation of the infection machinery.

4. MATERIALS AND METHODS

4.1 Fungal and bacterial strains used

We used the *Z. tritici* Swiss strain ST99CH_3D7 ((39); abbreviated as 3D7). All mutants were obtained either in 3D7 expressing the codon optimized version of the enhanced green fluorescent protein (eGFP) (3D7-GFP; (10, 40)), or in a mutant reporter line that expresses *mCherry* fused to His1 under the control of the *AvrStb6* promoter and located within the *AvrStb6* locus (10). Stellar *Escherichia coli* HST08 cells (Takara Bio, Japan) and the *Agrobacterium tumefaciens* strain AGL1 were used for cloning and *Z. tritici* transformation, respectively.

4.2 Bioinformatic tools

To identify and classify the KAT orthologues from *Z. tritici*, we first used the basic local alignment search tool (BLAST; (41)) from the National Centre for Biotechnology Information (NCBI) using the previously characterized KAT protein sequences from *S. cerevisiae* as queries (Table S1). Reverse BLAST was also performed to confirm that the identified protein sequences in *Z. tritici* were KAT orthologues. In parallel, we used the dbHiMo web-based data browser (26). Results obtained in the BLAST analysis were compared with results using dbHiMo to confirm that the same KATs were found in both cases. We obtained a multiple sequence alignment of the KAT orthologues (MUSCLE; (42)) and a phylogenetic tree. The protein sequences used for constructing the phylogenetic tree were obtained from NCBI (Table S2). Phylogenetic trees were constructed using the Molecular Evolutionary Genetics Analysis (MEGA-X 10.2; (43)) software, applying the maximum likelihood (ML) method with 1000 non-parametric bootstraps as statistical support. Trees were rooted using the midpoint rooting method. We edited the trees using the Interactive Tree Of Life (iTOL; (44)) software. Additionally, we identified protein domains in *Z. tritici* HMEs using HMMER (45) including all databases (Pfam, TIGRFAM, Gene3D, Superfamily, PIRSF and TreeFam) and represented the different protein domains using the R package “ragp” (46).

4.3 Generation of *Z. tritici* transformants

Plasmids for targeted gene deletion by homologous recombination were assembled using the In-Fusion® HD Cloning Kit (Takara Bio, Japan). Briefly, the nourseothricin resistance gene PCR-amplified from pES1-NAT-GFP (47) was flanked by homology arms of ca. 1 kb and inserted into the KpnI-SbfI-linearized acceptor plasmid pCGEN (48). Similarly, constructs for genetic complementation were generated by assembling gene sequences spanning from ca. 1 kb upstream of the start codon to right before the stop codon and the C-terminal 4xMyc-tag (49) into XhoI-linearized pLM1. Primers are listed in Table S3. *Z. tritici* gene deletion mutants and respective complementation mutants were obtained by *A. tumefaciens*-mediated transformation as previously described (10, 50) using nourseothricin (25 µg·mL^{-1}) and hygromycin (100 µg·mL^{-1}) for selection, respectively. Despite the presence of homology arms in the T-DNA, transformation of *Z. tritici* typically yields high frequencies of ectopic insertions by non-homologous end-joining instead of or in addition to targeted insertions by homologous recombination. To distinguish deletion mutants from ectopic insertion mutants, a PCR-based mutant screening was performed using either purified genomic DNA as template or directly adding liquid culture to the PCR reaction. The screening method includes a primer binding site present between the nourseothricin resistance gene and the downstream homology arm. The sequence of this screening primer binding site was chosen to match the sequence of the gene to be deleted in a way that yields two distinct amplicons in deletion and ectopic insertion mutants when combined with a primer binding site located in the region downstream of the homology arm (Figure S9). Since this screening method yields distinct amplicons for both deletion and ectopic insertion mutants, failed PCR reactions can easily be identified by the lack of both amplicons. Furthermore, the presence of both amplicons in the same reaction allows the identification of impure mutant lines and heterokaryons. Insertion copy numbers were determined by qPCR and mutant lines with multiple inserts were discarded. At least two independent lines were obtained per mutant and used for subsequent experiments.

4.4 Infection assays

Infection assays were performed on wheat (*Triticum aestivum* L.) plants of cultivar Runal grown for 15 days at 18°C during the day and 15°C during the night, with 16 hours of light and 65% of relative humidity. Sixteen seeds of cultivar Runal were sown in 11x11x12 cm pots with a peat-based substrate. Plants were fertilized after one week (Universal fertilizer, COMPO, Münster, Germany). The fungal inoculum was prepared one week before the infection by inoculating 50-100 µL of glycerol stock in 50 mL of on yeast extract-peptone-dextrose broth (YPD; yeast extract

399 10 g·L^{-1}; peptone 20 g·L^{-1}; dextrose 20 g·L^{-1}) amended with kanamycin (50 µg·mL^{-1}). Spore
400 suspensions were prepared as described (24) and quantified using a BLAUBRAND bright-line
401 Neubauer improved hemocytometer (0.100 mm depth, 0.0025 mm^2 area; Brand, Wertheim,
402 Germany), except for the ChIP-qPCR experiment in which we used the Spore Counter macro vs
403 2.13 (https://github.com/jalassim/SporeCounter.git; Julien Alassimone; ETH-Zürich,
404 Switzerland).

405 Wheat infection assays were performed using fungal suspensions at a concentration of 10^7
406 spores·mL^{-1} in 0.1% Tween-20 as previously described (24). Each pot was sprayed either with
407 12.5 mL 0.1% Tween-20 for mock treatment or 12.5 mL spore suspension for controls and
408 mutants. At least two independent mutant lines were used to evaluate symptom development
409 and pycnidia production. Symptoms produced by *Z. tritici* were analyzed on the second leaf at
410 two different time point using ImageJ (51) and an automated image analysis method (52). The
411 percentage of leaf aPLACL and pycnidia counts per square centimeter of lesion were used as
412 proxy for virulence and asexual reproduction, respectively.

413 4.5 Developmental assays

414 We performed fitness assays with *Z. tritici* mutants. A 3-µL drop of *Z. tritici* spore suspensions at
415 10^6, 10^5, 10^4 and 10^3 spores·mL^{-1} was placed on different types of media: YMA, YMA
416 supplemented with NaCl (0.5 M), H_2O_2 (1 mM), sorbitol (1 M), calcofluor white (200 ng·µL^{-1}), or
417 Congo red (2 mg·mL^{-1}); minimal medium (MM; Voguel's medium (53)), and MM supplemented
418 with fructose (5 g·L^{-1}), galactose (50 mM), GlcNAc (2.5 mM), or glucose (2.5 mM). Inoculated
419 agar plates were incubated at 18°C. An additional plate of YMA was incubated at 28°C. Pictures
420 were taken after 6 days.

421 Area of individual colonies of the mutants was estimated by inoculating ca. 100 colony-forming
422 units on YMA. Three independent replicates of each mutant were performed. After 5 days of
423 incubation at 18°C, pictures of the plates were taken, and the colony size was analyzed using
424 ImageJ.

425 4.6 Confocal laser scanning microscopy assays

426 Confocal assays were performed on a Zeiss LSM 880 super-resolution confocal microscope with
427 fast Airyscan. The emission settings were: 511 to 564 nm for the eGFP channel, 603 to 623 nm
428 for the mCherry channel, 460 to 480 nm for the mTurquoise2 channel and 692 to 697 nm for the
429 chloroplast detection. For excitation, an argon (488 nm) laser was used for track 1 (mCherry,
430 and chloroplasts) and a diode laser (405 nm) was used for track 2 (mTurquiose2 and eGFP).

Image processing was performed using Fiji (54) and included generation of maximum-intensity Z-projections for merging channels and addition of calibration bars. Colors were selected manually to facilitate channel identification. At least two independent lines per transformant were used. Experiments were performed at least twice.

4.7 Effector gene expression analysis

Axenically grown cultures obtained as described above were filtered through a nylon membrane and centrifuged at 5000 g, 4°C for 5 minutes. Supernatant was discarded and fungal pellets were ground in liquid N_2, using mortar and pestle. Infected plant tissue was collected at 6- and 10-days post infection (dpi). Eight centimeters of second leaves (after discarding 2 cm from the tip) were used for RNA extraction. Each replicate consisted of 2 leaves. At least three biological replicates were analyzed per treatment. RNA was extracted with Trizol (Life Technologies), purified (RNAeasy Mini Kit, QIAGEN Inc., The Netherlands) and treated with DNAse (QIAGEN Inc., The Netherlands). cDNA was synthesized by using the Primescript RT reagent kit (Takara Bio, Japan). qPCR was performed in a LightCycler480 II (Roche Diagnostics International AG, Rotkreuz, Switzerland) using the primers listed in Table S3, and data were analyzed with the LightCycler 480 software (Roche Diagnostics International AG, Rotkreuz, Switzerland) using *histone H3* (*3D7.g6784*) and *beta tubulin* (*3D7.g2064*) as reference genes. Relative fungal biomass *in planta* was calculated by dividing the transcript values of fungal housekeeping genes (histone H3 and beta tubulin) and the plant housekeeping gene *TaCDC48* (*Triticum aestivum* cell division control protein 48 homolog E-like; *Traes4A02G035500*) (55).

4.8 Chromatin extraction and immunoprecipitation (ChIP)

For *in vitro* chromatin extraction 150 mg of tissue were used, while for *in planta* chromatin extraction 250 mg of tissue were used. The micrococcal nuclease (M0247S; New England Biolabs, Ipswich, MA, USA) reaction was performed at 37°C for 20 minutes. Chromatin fixation, immunoprecipitation and de-crosslinking were performed as previously described (9, 10). Antibodies anti-H3 (ab1791, Abcam, Cambridge, UK), anti-H3K9ac (ab10812, Abcam, Cambridge, UK) and anti-H3K14ac (ab52946, Abcam, Cambridge, UK) were applied in 1:200 ratio. Subsequent qPCR was carried out on a LightCycler 480 instrument (Roche Diagnostics International AG, Rotkreuz, Switzerland). Acetylation levels were estimated as relative levels of H3K9ac and H3K14ac normalized to histone H3 as previously described (56, 57).

4.9 Statistics

Statistical analysis and graphic representations were performed using either RStudio version 1.4.1717 (58) or GraphPad Prism 8.0.2 for Windows (GraphPad Software, San Diego, California). For conducting the statistical analyses, Gaussian distribution of the data was tested using a Shapiro-Wilk normality test and homogeneity of variances was analyzed using a Brown-Forsythe test. If the data followed a normal distribution and preserved homoscedasticity, the parametric ordinary one-way ANOVA test was applied together with Fisher's LSD test (p-value < 0.05). If the aforementioned assumptions were not met, the non-parametric Kruskal-Wallis test was applied together with Dunn's uncorrected test (p-value < 0.05). In the case of ChIP data, two-way ANOVA and Bonferroni analyses were performed (p-value < 0.05). All raw data used for performing main text and supplementary figures are available in Dataset S1 and S2, respectively.

5. ACKNOWLEDGEMENTS

We would like to specially thank Javier Barrero, Pedro Crevillen and Jose Antonio Abelenda for their support and help with ChIP experiments and results interpretation. We would like to thank Thierry Marcel and Reda Amezrou for providing us with nonpublished information and to Julien Alassimone for providing us the Spore Counter macro. We thank Gero Steinberg for providing us with the vector containing the codon-optimized eGFP and 3D7-GFP, Jason Rudd for providing the vector PCGEN and Manuel Ene Ordorica for providing the 4xmyc sequence. We thank the Zymoseptoria laboratory at the CBGP for their help and support. We thank DSP Ltd (Delley, Switzerland) for providing us wheat seeds. The research was financed by the Ministry of Science and Innovation (Grant PID2019-108693RA-I00 financed by MICIN/AEI/ to AS-V). ASV was recipient of Ramon y Cajal grant RYC2018-025530-I of Spanish Ministry of Science, Innovation and Universities (MCIN/AEI/ and El FSE). MSF was recipient of Margarita Salas financed by the European Union - Next Generation EU (Grant MARSALAS21-31).

6. DATA AVALAIBILITY STATEMENT

The authors declare that the raw data of all the experiments are included in supplemental material (Datasets S1 and S2).

7. REFERENCES

1. Zeilinger S, Gupta VK, Dahms TES, Silva RN, Singh HB, Upadhyay RS, Gomes EV, Tsui CKM, Chandra Nayak S. 2016. Friends or foes? Emerging insights from fungal interactions with plants. FEMS Microbiol Rev 40:182.

2. Horbach R, Navarro-Quesada AR, Knogge W, Deising HB. 2011. When and how to kill a plant cell: infection strategies of plant pathogenic fungi. J Plant Physiol 168:51–62.

3. Rothbart SB, Strahl BD. 2014. Interpreting the language of histone and DNA modifications. Biochim Biophys Acta Gene Regul Mech 1839:627–643.

4. Strahl BD, David Allis C. 2000. The language of covalent histone modifications. Nature 403:41–45.

5. Möller M, Ridenour JB, Wright DF, Freitag M. 2022. H4K20me3 controls Ash1-mediated H3K36me3 and transcriptional silencing in facultative heterochromatin. bioRxiv 2022.11.25.517763.

6. Rando OJ, Winston F. 2012. Chromatin and transcription in yeast. Genetics 190:351–387.

7. Sterner DE, Berger SL. 2000. Acetylation of histones and transcription-related factors. Microbiology and Molecular Biology Reviews 64:435–459.

8. Freitag M. 2017. Histone methylation by SET domain proteins in fungi. Annu Rev Microbiol 71:413–439.

9. Soyer JL, Möller M, Schotanus K, Connolly LR, Galazka JM, Freitag M, Stukenbrock EH. 2015. Chromatin analyses of *Zymoseptoria tritici*: Methods for chromatin immunoprecipitation followed by high-throughput sequencing (ChIP-seq). Fungal Genetics and Biology 79:63–70.

10. Meile L, Peter J, Puccetti G, Alassimone J, McDonald BA, Sánchez-Vallet A. 2020. Chromatin dynamics contribute to the spatiotemporal expression pattern of virulence genes in a fungal plant pathogen. mBio 11:e02343-20.

11. Zhang W, Huang J, Cook DE. 2021. Histone modification dynamics at H3K27 are associated with altered transcription of *in planta* induced genes in *Magnaporthe oryzae*. PLoS Genet 17:e1009376.

12. Soyer JL, el Ghalid M, Glaser N, Ollivier B, Linglin J, Grandaubert J, Balesdent MH, Connolly LR, Freitag M, Rouxel T, Fudal I. 2014. Epigenetic control of effector gene expression in the plant pathogenic fungus *Leptosphaeria maculans*. PLoS Genet 10:e1004227.

13. Chujo T, Scott B. 2014. Histone H3K9 and H3K27 methylation regulates fungal alkaloid biosynthesis in a fungal endophyte-plant symbiosis. Mol Microbiol 92:413–434.

14. Lee KK, Workman JL. 2007. Histone acetyltransferase complexes: One size doesn't fit all. Nat Rev Mol Cell Biol 8:284–295.

15. González-Prieto JM, Rosas-Quijano R, Domínguez A, Ruiz-Herrera J. 2014. The *UmGcn5* gene encoding histone acetyltransferase from *Ustilago maydis* is involved in dimorphism and virulence. Fungal Genetics and Biology 71:86–95.

16. Nützmann HW, Reyes-Dominguez Y, Scherlach K, Schroeckh V, Horn F, Gacek A, Schümann J, Hertweck C, Strauss J, Brakhage AA. 2011. Bacteria-induced natural product formation in the fungus *Aspergillus nidulans* requires Saga/Ada-mediated histone acetylation. Proc Natl Acad Sci U S A 108:14282–14287.

17. Ma H, Li L, Gai Y, Zhang X, Chen Y, Zhuo X, Cao Y, Jiao C, Gmitter FG, Li H. 2021. Histone acetyltransferases and deacetylases are required for virulence, conidiation, DNA damage repair, and multiple stresses resistance of *Alternaria alternata*. Front Microbiol 12:783633.

18. Dubey A, Lee J, Kwon S, Lee YH, Jeon J. 2019. A MYST family histone acetyltransferase, MoSAS3, is required for development and pathogenicity in the rice blast fungus. Mol Plant Pathol 20:1491–1505.

19. Kong X, van Diepeningen AD, van der Lee TAJ, Waalwijk C, Xu J, Xu J, Zhang H, Chen W, Feng J. 2018. The *Fusarium graminearum* histone acetyltransferases are important for morphogenesis, DON biosynthesis, and pathogenicity. Front Microbiol 9:654.

20. Fones H, Gurr S. 2015. The impact of Septoria tritici Blotch disease on wheat: An EU perspective. Fungal Genetics and Biology 79:3–7.

21. Steinberg G. 2015. Cell biology of *Zymoseptoria tritici*: Pathogen cell organization and wheat infection. Fungal Genetics and Biology 79:17–23.

22. Sánchez-Vallet A, McDonald MC, Solomon PS, McDonald BA. 2015. Is *Zymoseptoria tritici* a hemibiotroph? Fungal Genetics and Biology 79:29–32.

23. Francisco CS, Ma X, Zwyssig MM, McDonald BA, Palma-Guerrero J. 2019. Morphological changes in response to environmental stresses in the fungal plant pathogen *Zymoseptoria tritici*. Sci Rep 9:1–18.

24. Meile L, Croll D, Brunner PC, Plissonneau C, Hartmann FE, McDonald BA, Sánchez-Vallet A. 2018. A fungal avirulence factor encoded in a highly plastic genomic region triggers partial resistance to septoria tritici blotch. New Phytologist 219:1048–1061.

25. Zhong Z, Marcel TC, Hartmann FE, Ma X, Plissonneau C, Zala M, Ducasse A, Confais J, Compain J, Lapalu N, Amselem J, McDonald BA, Croll D, Palma-Guerrero J. 2017. A small secreted protein in *Zymoseptoria tritici* is responsible for avirulence on wheat cultivars carrying the *Stb6* resistance gene. New Phytologist 214:619–631.

26. Choi J, Kim KT, Huh A, Kwon S, Hong C, Asiegbu FO, Jeon J, Lee YH. 2015. dbHiMo: a web-based epigenomics platform for histone-modifying enzymes. Database 8:2015:bav052.

27. Su C, Lu Y, Liu H. 2016. N-acetylglucosamine sensing by a GCN5-related N-acetyltransferase induces transcription via chromatin histone acetylation in fungi. Nat Commun 7:12916.

28. Brunner PC, Torriani SFF, Croll D, Stukenbrock EH, McDonald BA. 2013. Coevolution and life cycle specialization of plant cell wall degrading enzymes in a hemibiotrophic pathogen. Mol Biol Evol 30:1337–1347.

29. Palma-Guerrero J, Ma X, Torriani SFF, Zala M, Francisco CS, Hartmann FE, Croll D, McDonald BA. 2017. Comparative transcriptome analyses in *Zymoseptoria tritici* reveal

significant differences in gene expression among strains during plant infection. Molecular Plant-Microbe Interactions 30:231–244.

30. Roh TY, Ngau WC, Cui K, Landsman D, Zhao K. 2004. High-resolution genome-wide mapping of histone modifications. Nat Biotechnol 22:1013–1016.

31. Roh T-Y, Cuddapah S, Zhao K. 2005. Active chromatin domains are defined by acetylation islands revealed by genome-wide mapping. Genes Dev 19:542–52.

32. Amezrou R, Audéon C, Compain J, Gélisse S, Ducasse A, SAaintenac C, Lapalu N, Orford S, Croll D, Amselem J, Fillinger S, Marcel TC. 2022. A secreted protease-like protein in *Zymoseptoria tritici* is responsible for avirulence on Stb9 resistance gene in wheat. bioRxiv 2022.10.31.514577.

33. Soyer JL, Rouxel T, Fudal I. 2015. Chromatin-based control of effector gene expression in plant-associated fungi. Curr Opin Plant Biol 26:51–56.

34. Wang G, Song L, Bai T, Liang W. 2020. BcSas2-mediated histone H4K16 acetylation is critical for virulence and oxidative stress response of *Botrytis cinerea*. Molecular Plant-Microbe Interactions 33:1242–1251.

35. Karmodiya K, Krebs AR, Oulad-Abdelghani M, Kimura H, Tora L. 2012. H3K9 and H3K14 acetylation co-occur at many gene regulatory elements, while H3K14ac marks a subset of inactive inducible promoters in mouse embryonic stem cells. BMC Genomics 13:424.

36. Eberharter A, Becker PB. 2002. Histone acetylation: A switch between repressive and permissive chromatin. EMBO Rep 3:224–229.

37. Kalkhoven E, Teunissen H, Houweling A, Verrijzer CP, Zantema A. 2002. The PHD type zinc finger is an integral part of the CBP acetyltransferase domain. Mol Cell Biol 22:1961.

38. Clairet C, Gay EJ, Porquier A, Blaise F, Marais CL, Balesdent M-H, Rouxel T, Soyer JL, Fudal I. 2021. Regulation of effector gene expression as concerted waves in *Leptosphaeria maculans*: a two-players game. bioRxiv 2021.12.15.

39. Linde CC, Zhan J, McDonald BA. 2002. Population structure of *Mycosphaerella graminicola*: from lesions to continents. Phytopathology 92:946–955.

40. Kilaru S, Schuster M, Studholme D, Soanes D, Lin C, Talbot NJ, Steinberg G. 2015. A codon-optimized green fluorescent protein for live cell imaging in *Zymoseptoria tritici*. Fungal Genetics and Biology 79:125–131.

41. Altschul SF, Gish W, Miller W, Myers EW, Lipman DJ. 1990. Basic local alignment search tool. J Mol Biol 215:403–410.

42. Edgar RC. 2004. MUSCLE: multiple sequence alignment with high accuracy and high throughput. Nucleic Acids Res 32:1792–1797.

43. Tamura K, Stecher G, Kumar S. 2021. MEGA11: Molecular Evolutionary Genetics Analysis Version 11. Mol Biol Evol 38:3022–3027.

44. Letunic I, Bork P. 2021. Interactive tree of life (iTOL) v5: An online tool for phylogenetic tree display and annotation. Nucleic Acids Res 49:W293–W296.

608 45. Potter SC, Luciani A, Eddy SR, Park Y, Lopez R, Finn RD. 2018. HMMER web server: 2018
609 update. Nucleic Acids Res 46:W200–W204.

610 46. Dragićević MB, Paunović DM, Bogdanović MD, Todorović SI, Simonović AD. 2021. ragp:
611 Pipeline for mining of plant hydroxyproline-rich glycoproteins with implementation in
612 R. Glycobiology 30:19–35.

613 47. Meile L, Garrido-Arandia M, Bernasconi Z, Peter J, Schneller A, Bernasconi A,
614 Alassimone J, McDonald BA, Sánchez-Vallet A. 2022. Natural variation in *Avr3D1* from
615 *Zymoseptoria* sp. contributes to quantitative gene-for-gene resistance and to host
616 specificity. New Phytologist 10.1111/np.

617 48. Motteram J, Lovegrove A, Pirie E, Marsh J, Devonshire J, van de Meene A, Hammond-
618 Kosack K, Rudd JJ. 2011. Aberrant protein N-glycosylation impacts upon infection-
619 related growth transitions of the haploid plant-pathogenic fungus *Mycosphaerella*
620 *graminicola*. Mol Microbiol 81:415–433.

621 49. Evan GI, Lewis GK, Ramsay G, Bishop JM. 1985. Isolation of monoclonal antibodies
622 specific for human c-myc proto-oncogene product. Mol Cell Biol 5:3610–3616.

623 50. Zwiers LH, de Waard MA. 2001. Efficient *Agrobacterium tumefaciens*-mediated gene
624 disruption in the phytopathogen *Mycosphaerella graminicola*. Curr Genet 39:388–393.

625 51. Schneider CA, Rasband WS, Eliceiri KW. 2012. NIH Image to ImageJ: 25 years of image
626 analysis. Nature Methods 2012 9:7 9:671–675.

627 52. Stewart EL, Hagerty CH, Mikaberidze A, Mundt CC, Zhong Z, McDonald BA. 2016. An
628 improved method for measuring quantitative resistance to the wheat pathogen
629 *Zymoseptoria tritici* using high-throughput automated image analysis. Phytopathology
630 106:782–788.

631 53. Vogel HJ. 1956. A convenient growth medium for *Neurospora crassa*. Microbiology
632 Genetics Bulletin 13:42–43.

633 54. Schindelin J, Arganda-Carreras I, Frise E, Kaynig V, Longair M, Pietzsch T, Preibisch S,
634 Rueden C, Saalfeld S, Schmid B, Tinevez JY, White DJ, Hartenstein V, Eliceiri K,
635 Tomancak P, Cardona A. 2012. Fiji: an open-source platform for biological-image
636 analysis. Nat Methods 9:676–682.

637 55. King R, Urban M, Lauder RP, Hawkins N, Evans M, Plummer A, Halsey K, Lovegrove A,
638 Hammond-Kosack K, Rudd JJ. 2017. A conserved fungal glycosyltransferase facilitates
639 pathogenesis of plants by enabling hyphal growth on solid surfaces. PLoS Pathogens
640 13:e1006672.

641 56. Banerjee A, Mahata B, Dhir A, Mandal TK, Biswas K. 2019. Elevated histone H3
642 acetylation and loss of the Sp1–HDAC1 complex de-repress the GM2-synthase gene in
643 renal cell carcinoma. Journal of Biological Chemistry 294:1005–1018.

644 57. Liao L, Alicea-Velázquez NL, Langbein L, Niu X, Cai W, Cho EA, Zhang M, Greer CB, Yan
645 Q, Cosgrove MS, Yang H. 2019. High affinity binding of H3K14ac through collaboration
646 of bromodomains 2, 4 and 5 is critical for the molecular and tumor suppressor functions
647 of PBRM1. Mol Oncol 13:811–828.

58. Team Rs. 2020. RStudio team (2020). RStudio: Integrated development for R. RStudio, PBC, Boston, MA URL http://www.rstudio.com/.

8. TABLE

Table 1. Classification of lysine acetyltransferase (KAT) orthologues in *Zymoseptoria tritici* strain ST99CH_3D7.

KAT nomenclature	Previous nomenclature	KAT family	Gene ID in *Zymoseptoria tritici* strain ST99CH_3D7
KAT1	Hat1	GNAT	Not found
KAT2	Gcn5	GNAT	*3D7.g4775*
KAT5	Esa1	MYST	*3D7.g9281*
KAT6	Sas3	MYST	*3D7.g4263*
KAT8	Sas2	MYST	*3D7.g7031*
KAT9	Elp3	GNAT	*3D7.g8500*
KAT11	Rtt109	RTT109	*3D7.g8867*
-	Ngs1	GNAT	*3D7.g2851*

9. FIGURE LEGENDS

Figure 1. *Zymoseptoria tritici* has 3 lysine acetyltransferase (KAT) orthologues belonging to the MYST family (Esa1, Sas2 and Sas3) and 3 belonging to the GNAT family (Ngs1, Gcn5 and Elp3). A) Phylogenetic tree of the MYST family protein members from different fungal organisms. MYST sequences belonging to *Z. tritici* are indicated with orange dots. The protein names are colored according to their classification: Sas2 (KAT8; green), Esa1 (KAT5; orange), and Sas3 (KAT6; yellow). B) Phylogenetic tree of GNAT family proteins from different fungal organisms. GNAT sequences belonging to *Z. tritici* are indicated with blue dots. The protein names are colored according to the type of enzyme: Elp3 (KAT9; purple), Gcn5 (KAT2; light red), and Ngs1 (pink). The numbers below the branches represent the support values from 1000 bootstrap replicates using the maximum likelihood method. Trees have been rooted using the midpoint root method. Tree scale indicates branch length in the tree. Units are given in residue substitution per site. C) Domains identified in the KAT proteins of *Z. tritici*.

Figure 2. Specific regulation of *Z. tritici* lysine acetyltransferase (KAT) genes during infection. Expression levels of the KAT genes *Esa1* (MYST family), *Sas2* (MYST family), *Sas3* (MYST family), *Ngs1* (GNAT family), *Gcn5* (GNAT family), *Elp3* (GNAT family) and the effector genes *Avr3D1*, *AvrStb6* and *Mycgr3G76589* under axenic conditions in two media with different nutrient content: Yeast extract sucrose broth (YSB) and minimal medium (MM); and during infection at different time points (7-, 12-, 14- and 28-days post infection; dpi). Data were obtained from previously published RNA-seq studies (NCBI accessions: SRA SRP152081 and SRP077418) (23, 29). cpm: counts per million mapped reads.

Figure 3. **Acetylation levels of histone H3 lysine 9 (H3K9) and 14 (H3K14) in *Z. tritici* increase during plant infection.** Relative acetylation of H3K9 (A) and H3K14 (B) in 3D7-GFP *in vitro* and *in planta* in different regions of *AvrStb6*: 1000 base pairs (bp; -1000), 500 base pairs (-500), 300 bp (-300) and 50 bp (-50) upstream of the start codon, within the open reading frame (ORF), and 300 bp upstream of the start codon of *Avr3D1*. *TFIIIC* (100 bp upstream of start codon) was used as controls. Chromatin immunoprecipitation experiments were performed during host colonization at 11 days post infection (dpi). Acetylation levels are shown relative to H3 levels. Bars show the average of three independent biological replicates and the error bars represent the standard error of the mean. Asterisks indicate significant differences between infection and axenic conditions according to two-way ANOVA and Bonferroni tests ($p < 0.05$).

Figure 4. Lysine acetyltransferases (KATs) are involved in *Z. tritici* infection. Relative biomass to a reference control of the control (3D7-GFP) and the KAT mutants (Δ*Ngs1*, Δ*Sas2*, Δ*Sas3*,

686 Δ*Gcn5* and Δ*Elp3*) during infection at 10 days post infection (dpi) (A) and of 3D7-GFP and Δ*Sas3*
687 at 6 dpi (B). Representative pictures of wheat leaves infected with 3D7-GFP and the knockout
688 mutants in the KAT genes at 20 dpi (C). Percentage of leaf area covered by lesions (PLACL) at 17
689 dpi (D) and pycnidia per cm^2 of lesion at 20 dpi (E) of wheat plants infected with the control and
690 the KAT mutants. In A and B, black bars represent 3D7-GFP, dark grey bars represent MYST-
691 family mutants and light grey bars represent GNAT-family mutants. In D and E, green represents
692 3D7-GFP, orange represents MYST-family mutants and blue represents GNAT-family mutants.
693 Dashed lines represent the median, dotted lines represent first and third quartiles and black
694 dots represent individual data points. Asterisks indicate significant differences with 3D7-GFP
695 according to Kruskal-Wallis and Dunn's tests (* $p < 0.05$; ** $p < 0.01$; **** $p < 0.0001$).

696 **Figure 5. Lysine acetyltransferases (KATs) regulate effector gene expression under axenic**
697 **conditions.** Relative expression of *Avr3D1* (A) and *AvrStb6* (B) in the control (3D7-GFP) and the
698 KAT mutants grown on yeast-malt-sucrose agar (YMA) for 6 days. *β-tubulin* and *histone H3* were
699 used both as reference genes. Each bar corresponds to the mean expression value of 3 biological
700 replicates and error bars represent the standard error of the mean. Asterisks indicate statistical
701 differences with 3D7-GFP according to Kruskal-Wallis with uncorrected Dunn's tests. (* $p < 0.05$;
702 *** $p < 0.001$). Expression pattern of *AvrStb6* at the cellular level at 6 days post infection (dpi)
703 in the control reporter line (C); and the control reporter line lacking *Sas2* (D); *Sas3* (E); *Ngs1* (F);
704 *Gcn5* (G); and *Elp3* (H). In the reporter line, mCherry fused to histone 1 was expressed under the
705 control of the *AvrStb6* promoter in the *AvrStb6* locus. This allowed the localization of the
706 reporter to the nucleus (red dots) and therefore to monitor the activity of the *AvrStb6* promoter
707 at the single-cell level (10). Fungal blastospores are labelled with mTurquoise2 and shown in
708 yellow. Calibration bars correspond to 25 µm.

709 **Figure 6. Lysine acetyltransferases (KATs) are involved in effector gene regulation during plant**
710 **colonization.** Relative expression of *Avr3D1* (A), *AvrStb6* (B), *AvrStb9* (C) and *Mycgr3G76589* (D)
711 in the control (3D7-GFP) and KAT mutants (Δ*Ngs1*, Δ*Sas2*, Δ*Sas3*, Δ*Gcn5* and Δ*Elp3*) during wheat
712 infection at 10 days post infection (dpi). *β-tubulin* and *histone H3* were used both as reference
713 genes. Bars correspond to the mean expression value of 3 biological replicates per treatment
714 and error bars represent standard error of the mean. Asterisks indicate significant differences
715 with 3D7-GFP according to Kruskal-Wallis and Dunn's tests (* $p < 0.05$; ** $p < 0.01$). Expression
716 pattern of *AvrStb6* at the cellular level at 6 dpi in the E) control reporter line; and the control
717 reporter line lacking *Sas2* (F); *Sas3* (G); *Ngs1* (H); *Gcn5* (I); and *Elp3* (J). In the reporter line,
718 mCherry fused to histone 1 was expressed under the control of the *AvrStb6* promoter in the
719 *AvrStb6* locus. This allowed the localization of the reporter to the nucleus (red dots) and

720 therefore monitoring the activity of the *AvrStb6* promoter at the single-cell level (10). Fungal
721 hyphae are labelled with mTurquoise2 and shown in yellow. Chloroplasts are indicated in blue.
722 White discontinuous lines indicate the stomata. Hyphae penetrating the stomata are indicated
723 with an arrow. Calibration bars correspond to 25 µm.

724 **Figure 7. Histone H3 lysine 9 (H3K9) and 14 (H3K14) acetylation in effector genes is mediated**
725 **by Sas3 *in planta*.** Relative acetylation of H3K9 (A) and H3K14 (B) in the control (3D7-GFP) and
726 Δ*Sas3* in different regions of *AvrStb6*: 1000 base pairs (bp; -1000), 500 base pairs (-500), 300 bp
727 (-300) and 50 bp (-50) upstream the start codon; and in the open reading frame region (ORF).
728 We also evaluated the acetylation of these two marks 300 bp upstream of the starting codon of
729 *Avr3D1*. *TFIIIC* (100 bp upstream of start codon) was used as control. Chromatin
730 immunoprecipitation experiments were performed during host colonization at 11 dpi.
731 Acetylation levels are shown relative to H3 levels. Bars show the average of three independent
732 biological replicates and the error bars represent the standard error of the mean. Asterisks
733 indicate significant differences between Δ*Sas3* and 3D7-GFP according to two-way ANOVA and
734 Bonferroni tests ($p < 0.05$).

735 **9. SUPPLEMENTAL MATERIAL TABLES**

736 **Table S1. BLASTp analysis identify 5 lysine acetyltransferases (KATs) from the MYST and GNAT**
737 **families in *Z. tritici*.** KATs of *Saccharomyces cerevisiae* used, query cover, E-value, percentage of
738 identity, accession number and gene ID of the best hit in *Z. tritici* are indicated.

***S. cerevisiae* KAT**	**Query Cover**	**E- value**	**Percentage of Identity**	**Accession (*Z. tritici*)**	**Associated *Z. tritici* gene ID**
Gcn5	80%	2e-164	60.76%	SMQ49624.1	*3D7.g4775*
Elp3	99%	0.0	74.24%	SMQ53347.1	*3D7.g8500*
Sas2	60%	1e-46	39.71%	SMQ51878.1	*3D7.g7031*
Sas3	47%	9e-79	36.83%	SMQ49112.1	*3D7.4263*
Esa1	99%	5e-162	49.41%	SMQ54127.1	*3D7.9281*

739

740 **Table S2. NCBI accession numbers used for performing the phylogenetic tree.**

KAT	Organism	NCBI accession number
Ngs1	*Neurospora crassa*	CAE85548.1
Ngs1	*Fusarium oxysporum*	KAF6521047.1
Ngs1	*Trichoderma reesei*	XP_006966911.1
Ngs1	*Aspergillus fumigatus*	KAH3100114.1
Ngs1	*Histoplasma capsulatum*	QSS62698.1
Ngs1	*Zymoseptoria tritici*	SMQ47703
Ngs1	*Candida albicans*	AOW30790.1
Sas2	*Saccharomyces cerevisiae*	DAA10024.1
Sas2	*Fusarium oxysporum*	SCO82216.1
Sas2	*Kluyveromyces marxianus*	XP_022675924
Sas2	*Beauveria bassiana*	KAF1731046.1
Sas2	*Zygosaccharomyces mellis*	GCE98240.1
Sas2	*Fusarium graminearum*	XP_011324667.1
Sas2	*Zymoseptoria tritici*	SMQ51878 .1
Sas3	*Saccharomyces cerevisiae*	DAA07067.1
Sas3	*Fusarium graminearum*	XP_011320283.1
Sas3	*Metarhizium robertsii*	XP_007818471.1
Sas3	*Fusarium oxysporum*	EWZ39814.1
Sas3	*Magnaphorte oryzae*	XP_003713627.1
Sas3	*Zymoseptoria tritici*	SMQ49112.1
Esa1	*Saccharomyces cerevisiae*	DAA11012.1
Esa1	*Magnaphorte oryzae*	XP_003719696.1
Esa1	*Fusarium graminearum*	Q4IEV4.1
Esa1	*Neurospora crassa*	XP_962217.1
Esa1	*Zymoseptoria tritici*	SMQ54127.1
Gcn5	*Saccharomyces cerevisiae*	DAA07067.1
Gcn5	*Ustylago maydis*	CAC80426.1
Gcn5	*Fusarium oxysporum*	EWZ52160.1
Gcn5	*Neurospora crassa*	XP_001728480.2
Gcn5	*Schizosaccharomyces pombe*	Q9UUK2.1
Gcn5	*Zymoseptoria tritici*	SMQ49624.1
Elp3	*Saccharomyces cerevisiae*	DAA11347.1
Elp3	*Fusarium graminearum*	XP_011317913.1
Elp3	*Magnaphorte oryzae*	XP_003710346.1
Elp3	*Schizosaccharomyces pombe*	NP_594862.1
Elp3	*Fusarium oxisporum*	XP_018239078.1
Elp3	*Candida albicans*	KAF6072097.1
Elp3	*Zymoseptoria tritici*	SMQ53347.1

741

742 **Table S3. Primers used in this work.**

Primer name	Primer sequence	Purpose
ASV18p_IF_KO-HAT_SAS2_F5	TAATTAAGATATCGAGCTCGGTGAGATCCTCGTAGTAGTCGT	Construct-KO-HAT_SAS2 with ASV19p
ASV19p_IF_KO-HAT_SAS2_R5	GGAGATGTGGAGTGGGGAGTGATTGCATTGAAACGG	Construct-KO-HAT_SAS2 with ASV18p
ASV20p_NAT_F	CCCACTCCACATCTCCACTC	Construct-KO-HAT_NAT Amplification with ASV21p
ASV21p_NAT_R	CCTCTTCGCTATTACGCCAG	Construct-KO-HAT_NAT Amplification with ASV20p
ASV22p_IF_KO-HAT_SAS2_F3	CGTAATAGCGAAGAGGCATCTCACTCATCTCACTCTCCACCGACATTGTTTCCGACTG	Construct-KO-HAT_SAS2 with ASV23p
ASV23p_IF_KO-HAT_SAS2_R3	CAGTGCCAAGCTTGCATGCCGTTTCCGTTCAACACAGCCT	Construct-KO-HAT_SAS2 with ASV22p
ASV24p_SAS2_ScreenP_F	CATCTCACTCATCTCACTCTC	Primer for screening KO-HAT_SAS2 with ASV25p
ASV25p_SAS2_ScreenP_R	GGATACGCAATGAACTTCTGG	Primer for screening KO-HAT_SAS2 with ASV24p
ASV26p_IF_KO-HAT_NGS1_F5	GCCGAATTCGAGCTCGGGTGTGGTGGAAACTCTCCC	Construct KO-HAT_NGS1 with ASV27p
ASV27p_IF_KO-HAT_NGS1_R5	GGAGATGTGGAGTGGGTTTGCATGGATTTGAGGAGGT	Construct KO-HAT_NGS1 with ASV26p
ASV28p_IF_KO-HAT_NGS1_F3	CGTAATAGCGAAGAGGGATTCCTCACATTCGTCAACACCATCCTGCTGGCACTATTGG	Construct KO-HAT_NGS1 with ASV29p
ASV29p_IF_KO-HAT_NGS1_R3	TAAAGCTTGCATGCCGCGATACTTCCTCACTACCC	Construct KO-HAT_NGS1 with ASV28p
ASV30p_KO-HAT_NGS1_ScreenP_F	GATTCCTCACATTCGTCAACAC	Primer for screening KO-HAT_NGS1 with ASV31p
ASV31p_KO-HAT_NGS1_ScreenP_R	ACTTCTTCTCGCTACCTCCTG	Primer for screening KO-HAT_NGS1 with ASV30p
ASV38p_KO-HAT_SAS3_F5	GCCGAATTCGAGCTCGGGTCAAGGCGATGTATTTCC	Construct KO-HAT_SAS3 with ASV39p
ASV39p_KO-HAT_SAS3_R5	GGAGATGTGGAGTGGGCATGTTGGTGGTTGAACTTGAG	Construct KO-HAT_SAS3 with ASV38p
ASV40p_KO-HAT_SAS3_F3	CGTAATAGCGAAGAGGCTTGAAATCATGTGGCTCGTGGTTGTGCCTTGTAATTCACGCC	Construct KO-HAT_SAS3 with ASV41p
ASV41p_KO-HAT_SAS3_R3	TAAAGCTTGCATGCCAATGCCTTGGTCGCTTTCCT	Construct KO-HAT_SAS3 with ASV40p
ASV42p_ScreenP_SAS3KO-HAT_F	CTTGAAATCATGTGGCTCGTGG	Primer for screening KO-HAT_SAS3 with ASV43p
ASV43p_ScreenP_SAS3KO-HAT_R	GCCTTCGTGTTGTCTGTCTG	Primer for screening KO-HAT_SAS3 with ASV42p
ASV44p_KO-HAT_GCN5_F5	GCCGAATTCGAGCTCGGGAGGTGGAGTGTAGGTATAGG	Construct KO-HAT_GCN5 with ASV45p
ASV45p_KO-HAT_GCN5_R5	GGAGATGTGGAGTGGGAGAGCGAGGTCAAGTTGTGAG	Construct KO-HAT_GCN5 with ASV44p
ASV46p_KO-HAT_GCN5_F3	CGTAATAGCGAAGAGGAGTGAAGAAGCCTCCAGCAGGAATTACAAGCTTGGCTCAC	Construct KO-HAT_GCN5 with ASV47p
ASV47p_KO-HAT_GCN5_R3	TAAAGCTTGCATGCCAATGCGCGGTATTGATTGAG	Construct KO-HAT_GCN5 with ASV46p
ASV48p_ScreenP_GCN5KO-HAT_F	AGTGAAGAAGCCTCCAGCAG	Primer for screening KO-HAT_GCN5 with ASV49p
ASV49p_ScreenP_GCN5KO-HAT_R	TATACCTCTCCTCGCCACTC	Primer for screening KO-HAT_GCN5 with ASV48p
ASV50p_KO-HAT_ELP3KO-HAT_F5	GCCGAATTCGAGCTCGCGCCAAAGCAGTGATCAACG	Construct KO-HAT_ELP3 with ASV51p

ASV51p_KO-HAT_ELP3KO-HAT_R5	GGAGATGTGGAGTGGGATTGAGCAATGCCGACTGTG	Construct KO-HAT_ELP3 with ASV50p
ASV52p_KO-HAT_ELP3KO-HAT_F3	CGTAATAGCGAAGAGGGTGTGAGACGACCTTGAATCCAGGTCCTGGAGGTGTTGTAGC	Construct KO-HAT_ELP3 with ASV53p
ASV53p_KO-HAT_ELP3KO-HAT_R3	TAAAGCTTGCATGCCGAAATTAGATGTAATCAAGCCCGC	Construct KO-HAT_ELP3 with ASV52p
ASV54p_ScreenP_ELP3KO-HAT_F	GTGTGAGACGACCTTGAATCCA	Primer for screening KO-HAT_ELP3 (ASV12) with ASV55p
ASV55p_ScreenP_ELP3KO-HAT_R	CCCTATTTGAGATTGCGTGTCAG	Primer for screening KO-HAT_ELP3 (ASV12) with ASV54p
ASVp158_Myc_R	AAATCGAATGTCCGCCTCGACTATAGGTCCTCTTCAGAAATAAGTTTT	Primer for construction of complementations with myc tag
ASVp165_Gcn5c_F	AATTAAGATATCGAGCTCGAAGGAGTAGGAGAATCTGGCG	Primer for construction of complementations of Gcn5
ASVp166_Gcn5_C_R	ACTTTTGTTCCTCAGGCTGCCGATTTGTCG	Primer for construction of complementations of Gcn5
ASVp167_Gcn5_Myc_F	GCAGCCTGAGGAACAAAAGTTGATCTCTGAAGAGG	Primer for construction of complementations of Gcn5 + myc
ASVp193_SAS3_C_F	AATTAAGATATCGAGCTCGAAGGACGTACGGCGGTGCAG	Primer for construction of complementations of Sas3
ASVp194_SAS3_C_R	ACTTTTGTTCCTCATACTGGATCTCGTCATCCTCC	Primer for construction of complementations of Sas3
ASVp195_SAS3_myc_F	CCAGTATGAGGAACAAAAGTTGATCTCTGAAGAGG	Primer for construction of complementations of Sas3
ASVp204_SAS3_C_F2	AATTAAGATATCGAGCTCGACCTTGGTCGCTTTCCTCCATTT	Primer for construction of complementations of Sas3
ASVp205_SAS3_C_F3	AATTAAGATATCGAGCTCGAGCCTTCGTGTTGTCTGTCTG	Primer for construction of complementations of Sas3
ASVp206_SAS3_C_F4	AATTAAGATATCGAGCTCGATCCAGCACGTACTCTGCTTATC	Primer for construction of complementations of Sas3
ASVp207_SAS3_C_R2	AATTAAGATATCGAGCTCGATGGTTGAGGTGTTCGGAAGG	Primer for construction of complementations of Sas3
ASVp208_SAS3_C_R3	AATTAAGATATCGAGCTCGAGCCGAAGAACTAGATCGTGGAG	Primer for construction of complementations of Sas3
ASVp219_AvrStb9_q1F	GCTTCGTGAGCGTGAATGAC	Primer for amplification of AvrStb9 in qPCR
ASVp220_AvrStb9_q1R	GACGGATCGAGGTACCGAAC	Primer for amplification of AvrStb9 in qPCR
ASVp221_AvrStb9_q2F	CTCGTATTTGCTTCCTCCGC	Primer for amplification of AvrStb9 in qPCR
ASVp222_AvrStb9_q2R	ATCAAGTCCAAGGTGTCGGT	Primer for amplification of AvrStb9 in qPCR
ASVp225_LM160_TFIIIC_qF1	AGAGGGGTCCGTTCATCTCA	Transcription factor III - Reference gene for ChIP-qPCR
ASVp226_LM161_TFIIIC_qR1	GTCGAAGCAGTAGAGGCGTT	Transcription factor III - Reference gene for ChIP-qPCR
ASVp232_H3_F1	TCGCAAGTCCGCACCATCCA	Histone H3 - Housekeeping gene for qPCR
ASVp232_H3_F1	TCGCAAGTCCGCACCATCCA	Histone H3 - Housekeeping gene for qPCR
ASVp238_B-Tub_F2	GAGGAGTTCCCCGACCGCAT	Beta tubulin - Housekeeping gene for qPCR
ASVp239_B-Tub_R2	AGCTGGTGGACGGAGAGGGT	Beta tubulin - Housekeeping gene for qPCR
ASVp242_AvrStb6_1000_ChIPqF	TCCCTGTCCGGAAACTAGGA	Primer for amplification of 1000 bp upstream of AvrStb6 in ChIP-qPCR
ASVp243_AvrStb6_1000_ChIPqR	GGGCCTGCTTAATAAATGGCG	Primer for amplification of 1000 bp upstream of AvrStb6 in ChIP-qPCR

ASVp246_AvrStb6_500_ChIPqF	TTTCCGGCACTTGCCTAACT	Primer for amplification of 500 bp upstream of AvrStb6 in ChIP-qPCR
ASVp247_AvrStb6_500_ChIPqR	TCCGCGCTATTCCTGTATGC	Primer for amplification of 500 bp upstream of AvrStb6 in ChIP-qPCR
ASVp250_AvrStb6_300_ChIPqF	CCAGGGGCTATGCACTACTT	Primer for amplification of 300 bp upstream of AvrStb6 in ChIP-qPCR
ASVp251_AvrStb6_300_ChIPqR	CGGCTCCTGCACCCAAAATA	Primer for amplification of 300 bp upstream of AvrStb6 in ChIP-qPCR
ASVp252_AvrStb6_50_ChIPqF	CTCAACCAAGACCAAAGCAGC	Primer for amplification of 50 bp upstream of AvrStb6 in ChIP-qPCR
ASVp253_AvrStb6_50_ChIPqR	AATGGATTCGGCGACAGGTG	Primer for amplification of 50 bp upstream of AvrStb6 in ChIP-qPCR
ASVp256_AvrStb6_ORF_ChIPqF	ATAGATCTCTGCAAGGCGGG	Primer for amplification of ORF of AvrStb6 in ChIP-qPCR
ASVp257_AvrStb6_ORF_ChIPqR	ACACCTTGGATATTGCCCGT	Primer for amplification of ORF of AvrStb6 in ChIP-qPCR
ASVp258_1qPCR_AvrStb6_fw (LM254)	AAGGCGGGTCCTAGTTGCT	Primer for amplification of AvrStb6 in qPCR
ASVp259_1qPCR_AvrStb6_rv (LM255)	AAGCTGCTGTGATGGAGAGC	Primer for amplification of AvrStb6 in qPCR
LM170_581_qF2	AGCATTCGACGACTGTTGGT	Primer for Avr3D1 amplification with LM171 in ChIP-qPCR
LM171_581_qR2	GGTGGCTAGCTTGGAACTGT	Primer for Avr3D1 amplification with LM170 in ChIP-qPCR
LM288_Cellulase_qF4	AACCAATACGGCGTCCAGA	Primer for Mycgr3G76589 qPCR amplification with LM289
LM289_Cellulase_qR4	CCACTCCTGCTCACCAAGTC	Primer for Mycgr3G76589 qPCR amplification with LM288
LM343B_NATqF	AGGTCACCAACGTCAACG	Primer for Copy number of resistant cassete (natR) with LM344B
LM344B_NATqR	CTCATGTAGAGCGCCAGC	Primer for Copy number of resistant cassete (natR) with LM343B
CDC48_QPCR_F2	GTCCTCCTGGCTGTGGTAAAAC	Primer for amplification of cell division control 48 gene in wheat
CDC48_QPCR_R2	AGCAGCTCAGGTCCCTTGATAC	Primer for amplification of cell division control 48 gene in wheat

743

10. SUPPLEMENTAL MATERIAL FIGURE LEGENDS

Figure S1. Sas3, Sas2 and Gcn5 regulate growth and development of *Z. tritici.* Colony area of the control (3D7-GFP), Δ*Ngs1*, Δ*Sas2*, Δ*Sas3*, Δ*Gcn5* and Δ*Elp3* grown for 5 days on yeast-malt-sucrose agar (YMA). Green bar represents 3D7-GFP, orange bars represent MYST-family mutants and blue bars represent GNAT-family mutants. Bars represent average of three independent biological replicates and error bars represent the standard error of the mean. A representative image of colonies of each mutant is shown. Additionally, an amplification of a colony of the control and Δ*Sas2* are shown. Asterisks indicate significant differences with 3D7-GFP according to Kruskal-Wallis and uncorrected Dunn's tests ($p < 0.05$).

Figure S2. Lysine acetyltransferases (KATs) are not positive regulators of stress tolerance. Three µL of fungal spore suspensions at a concentration of 10^6, 10^5, 10^4 and 10^3 spores·mL^{-1} of the controls (3D7 and 3D7-GFP), Δ*Ngs1*, Δ*Sas2*, Δ*Sas3*, Δ*Gcn5* and Δ*Elp3* were inoculated. Media used were yeast-malt-sucrose agar (YMA); YMA supplemented with NaCl (0.5 M), H_2O_2 (1 mM), sorbitol (1 M), Calcofluor white (200 ng·µL^{-1}) or Congo red (2 mg·mL^{-1}); minimal medium (MM; Voguel's), MM supplemented with fructose (5 g·L^{-1}), galactose (50 mM), GlcNAc (2.5 mM), or glucose (2.5 mM). Plates were incubated at 18°C for 6 days. One additional plate of YMA was incubated at 28°C.

Figure S3. Infection assays of at least two independent mutant lines of lysine acetyltransferases (KATs) from the MYST family. Percentage of leaf area covered by lesions (PLACL) at 14 days post infection (dpi) (A) and at 20 dpi (B) and pycnidia per cm^2 lesion at 14 dpi (C) and 20 dpi (D) in the three independent Δ*Sas2* lines (#1, #2, #3). PLACL at 14 dpi (E) and 20 dpi (F) and pycnidia per cm^2 lesion at 14 dpi (G) and at 20 dpi (H) of two independent Δ*Sas3* mutant lines (#1, #2). Dashed lines represent the median, dotted lines represent first and third quartiles and black dots represent individual data points. Asterisks indicate statistically significant differences with the control (3D7-GFP) according to Kruskal-Wallis non-parametric statistical and posthoc uncorrected Dunn's tests (* $p < 0.05$; ** $p < 0.01$; *** $p < 0.001$; **** $p < 0.0001$).

Figure S4. Infection assays of three independent mutant lines of lysine acetyltransferases (KATs) from the GNAT family. Percentage of leaf area covered by lesions (PLACL) at 15 days post infection (dpi) (A) and at 20 dpi (B) and pycnidia per cm^2 lesion at 15 dpi (C) and 20 dpi (D) in three Δ*Ngs1* independent lines (#1, #2, #3). PLACL at 15 dpi (E) and 21 dpi (F) and pycnidia per cm^2 lesion at 15 dpi (G) and at 21 dpi (H) of three independent lines of Δ*Gcn5* (#1, #2, #3). PLACL at 14 dpi (I) and 23 dpi (J) and pycnidia per cm^2 lesion at 14 dpi (K) and at 23 dpi (L) of three

777 independent lines of Δ*Elp3* (#1, #2, #3). Dashed lines represent the median, dotted lines
778 represent first and third quartiles and black dots represent individual data points. Asterisks
779 indicate statistically significant differences with 3D7-GFP according to the Kruskal-Wallis non-
780 parametric statistical and posthoc uncorrected Dunn's tests (* $p < 0.05$; ** $p < 0.01$; *** $p <$
781 0.001; **** $p < 0.0001$).

782 **Figure S5. Fungal biomass of Δ*Sas3* and Δ*Gcn5*.** Relative fungal biomass of the control (3D7-
783 GFP), two independent lines of Δ*Sas3* and three independent lines of Δ*Gcn5* at 6 days post
784 infection (dpi). Bars correspond to the average of three biological replicates. Error bars
785 represent the standard error of the mean. No significant differences with 3D7-GFP according to
786 the Kruskal-Wallis test were identified ($p < 0.05$).

787 **Figure S6. Δ*Sas2*, Δ*Sas3* and Δ*Gcn5* produce anormal macroscopic disease symptoms.**
788 Amplified pictures of leaves (length 14 cm) infected by 3D7-GFP (A), Δ*Sas2* (B), Δ*Sas3* (C) and
789 Δ*Gcn5* (D) at 20 days post infection. Red/orange/yellow symptoms produced in the wheat
790 cultivar Runal by the mutants are indicated with colored arrows. Note that no pycnidia were
791 produced by Δ*Sas3* and Δ*Gcn5* in the spots with red/orange/yellow symptoms.

792 **Figure S7. Complementation of Δ*Sas3* and Δ*Gcn5* recover the virulence phenotype.** Percentage
793 of leaf area covered by lesions (A) and pycnidia per cm^2 of lesion (B) at 17 days post infection
794 (dpi). Dashed lines represent the median, dotted lines represent first and third quartiles and
795 black dots represent individual data points. Asterisks indicate statistically significant differences
796 with 3D7-GFP according to the Kruskal-Wallis non-parametric statistical and posthoc
797 uncorrected Dunn's tests (* $p < 0.05$; ** $p < 0.01$; **** $p < 0.0001$).

798 **Figure S8. The expression pattern of *Mycgr3G76589* is not altered in lysine acetyltransferase**
799 **(KAT) mutants under axenic conditions**. Relative expression of *Mycgr3G76589* in 3D7-GFP and
800 the KATs mutants grown on yeast-malt-sucrose agar (YMA) for 6 days. Tubulin and histone H3
801 were used as reference genes. Each bar corresponds to the average of 3 biological replicates.
802 Error bars represent the standard error of the mean. No significant differences with 3D7-GFP
803 according to the Kruskal-Wallis test were found ($p < 0.05$).

804 **Figure S9. PCR screening strategy to identify gene deletion mutants.** Top: Blue crosses
805 represent homologous recombination events during fungal transformation. The forward
806 screening primer binding sites within the gene of interest and the T-DNA are identical. Sizes of
807 different parts do not correspond to a specific construct used in this study. Bottom: Example
808 screening results for Δ*Elp3* mutant lines using liquid cultures directly added to the reaction. PCRs

809 using forward and reverse screening primers yield distinct amplicons for native genes (1967 bp)

810 and disrupted genes (1058 bp). Each lane represents a different mutant line.

A

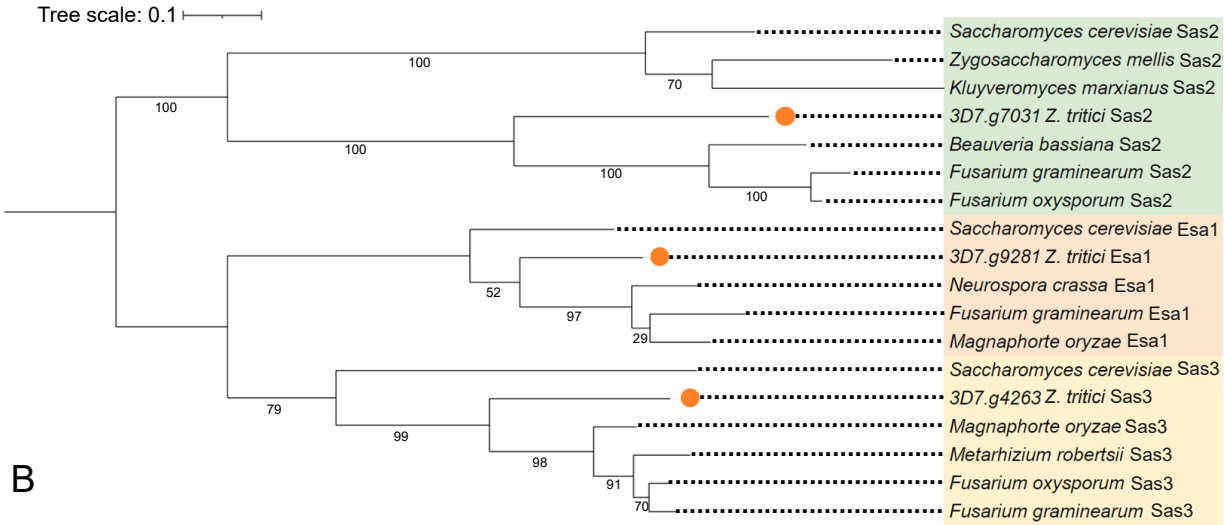
Tree scale: 0.1
Saccharomyces cerevisiae Sas2
Zygosaccharomyces mellis Sas2
Kluyveromyces marxianus Sas2
3D7.g7031 Z. tritici Sas2
Beauveria bassiana Sas2
Fusarium graminearum Sas2
Fusarium oxysporum Sas2
Saccharomyces cerevisiae Esa1
3D7.g9281 Z. tritici Esa1
Neurospora crassa Esa1
Fusarium graminearum Esa1
Magnaphorte oryzae Esa1
Saccharomyces cerevisiae Sas3
3D7.g4263 Z. tritici Sas3
Magnaphorte oryzae Sas3
Metarhizium robertsii Sas3
Fusarium oxysporum Sas3
Fusarium graminearum Sas3

B

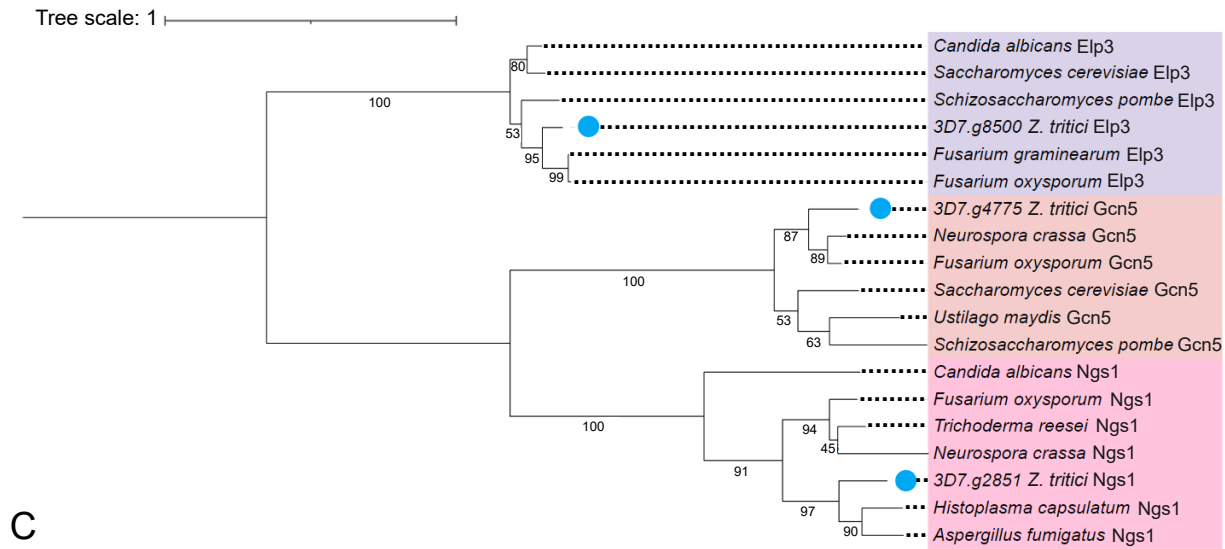
Tree scale: 1
Candida albicans Elp3
Saccharomyces cerevisiae Elp3
Schizosaccharomyces pombe Elp3
3D7.g8500 Z. tritici Elp3
Fusarium graminearum Elp3
Fusarium oxysporum Elp3
3D7.g4775 Z. tritici Gcn5
Neurospora crassa Gcn5
Fusarium oxysporum Gcn5
Saccharomyces cerevisiae Gcn5
Ustilago maydis Gcn5
Schizosaccharomyces pombe Gcn5
Candida albicans Ngs1
Fusarium oxysporum Ngs1
Trichoderma reesei Ngs1
Neurospora crassa Ngs1
3D7.g2851 Z. tritici Ngs1
Histoplasma capsulatum Ngs1
Aspergillus fumigatus Ngs1

C

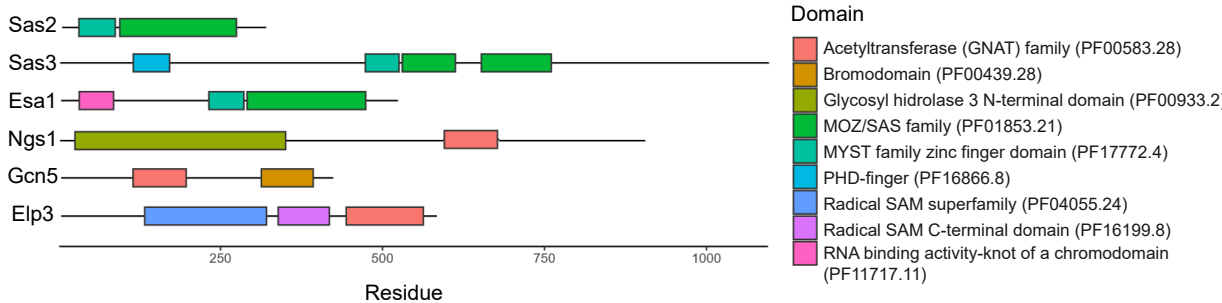
Sas2
Sas3
Esa1
Ngs1
Gcn5
Elp3
250
500
750
1000
Residue
Domain
Acetyltransferase (GNAT) family (PF00583.28)
Bromodomain (PF00439.28)
Glycosyl hidrolase 3 N-terminal domain (PF00933.2)
MOZ/SAS family (PF01853.21)
MYST family zinc finger domain (PF17772.4)
PHD-finger (PF16866.8)
Radical SAM superfamily (PF04055.24)
Radical SAM C-terminal domain (PF16199.8)
RNA binding activity-knot of a chromodomain (PF11717.11)

Figure 2

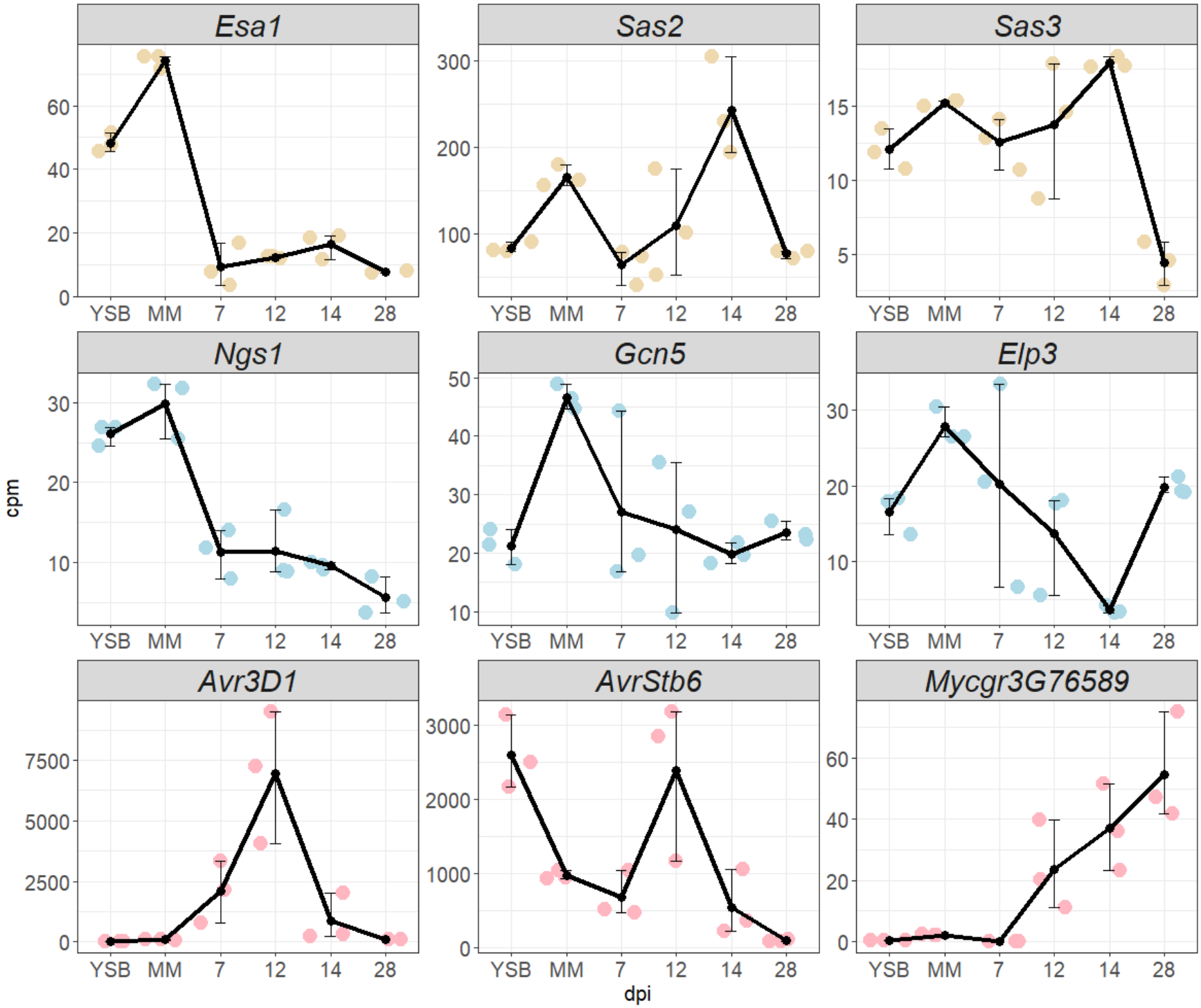
Esa1
Sas2
Sas3
Ngs1
Gcn5
Elp3
Avr3D1
AvrStb6
Mycgr3G76589
cpm
dpi
YSB
MM
7
12
14
28

A

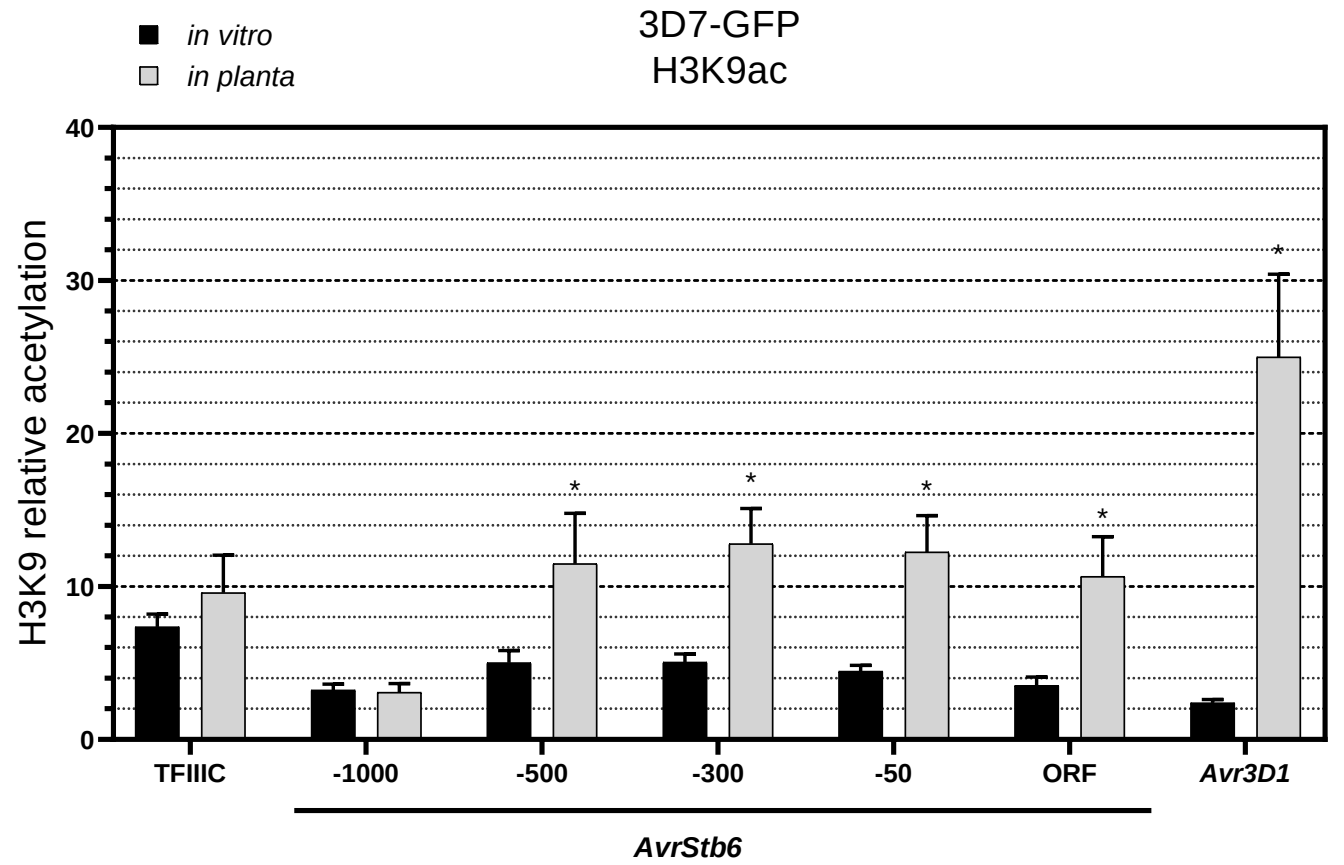
in vitro
in planta
3D7-GFP
H3K9ac
H3K9 relative acetylation
40
30
20
10
0
*
TFIIIC
-1000
-500
-300
-50
ORF
Avr3D1
AvrStb6

B

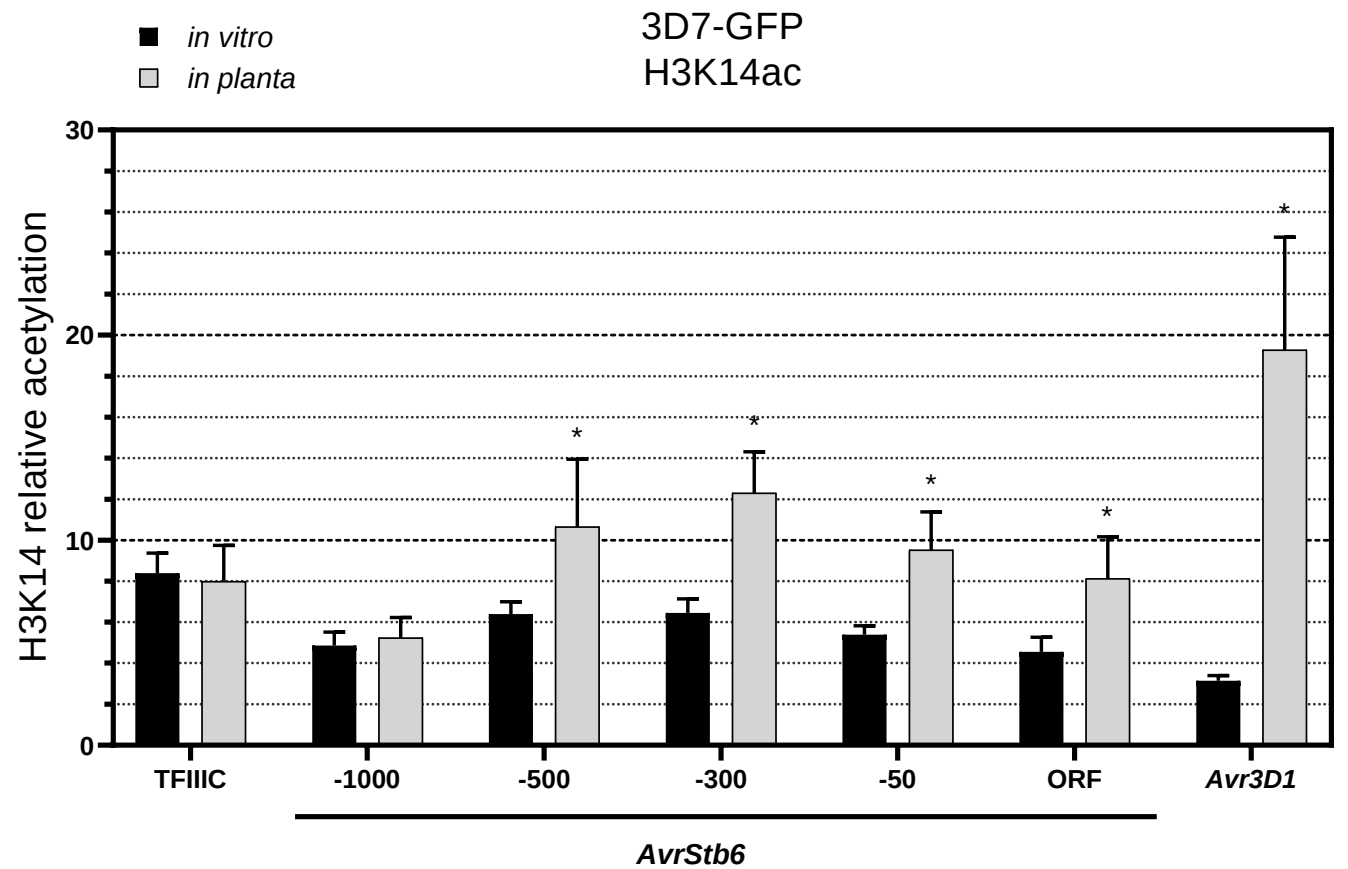
in vitro
in planta
3D7-GFP
H3K14ac
H3K14 relative acetylation
30
20
10
0
*
TFIIIC
-1000
-500
-300
-50
ORF
Avr3D1
AvrStb6

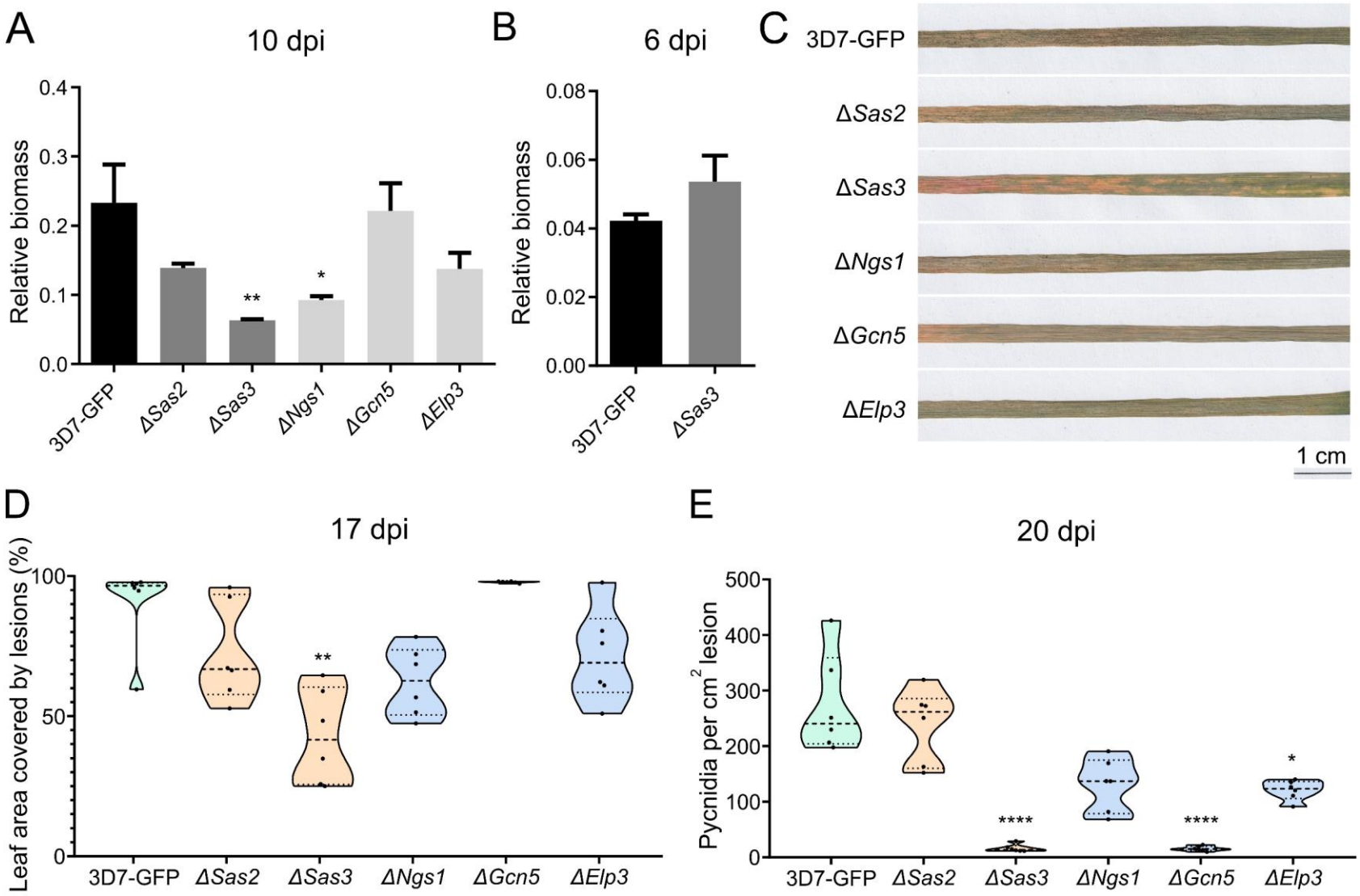
A
10 dpi
Relative biomass
0.4
0.3
0.2
0.1
0.0
**
*
3D7-GFP
ΔSas2
ΔSas3
ΔNgs1
ΔGcn5
ΔElp3
B
6 dpi
Relative biomass
0.08
0.06
0.04
0.02
0.00
3D7-GFP
ΔSas3
C
3D7-GFP
ΔSas2
ΔSas3
ΔNgs1
ΔGcn5
ΔElp3
1 cm
D
17 dpi
Leaf area covered by lesions (%)
100
50
0
**
3D7-GFP
ΔSas2
ΔSas3
ΔNgs1
ΔGcn5
ΔElp3
E
20 dpi
Pycnidia per cm2 lesion
500
400
300
200
100
0
****
****
*
3D7-GFP
ΔSas2
ΔSas3
ΔNgs1
ΔGcn5
ΔElp3

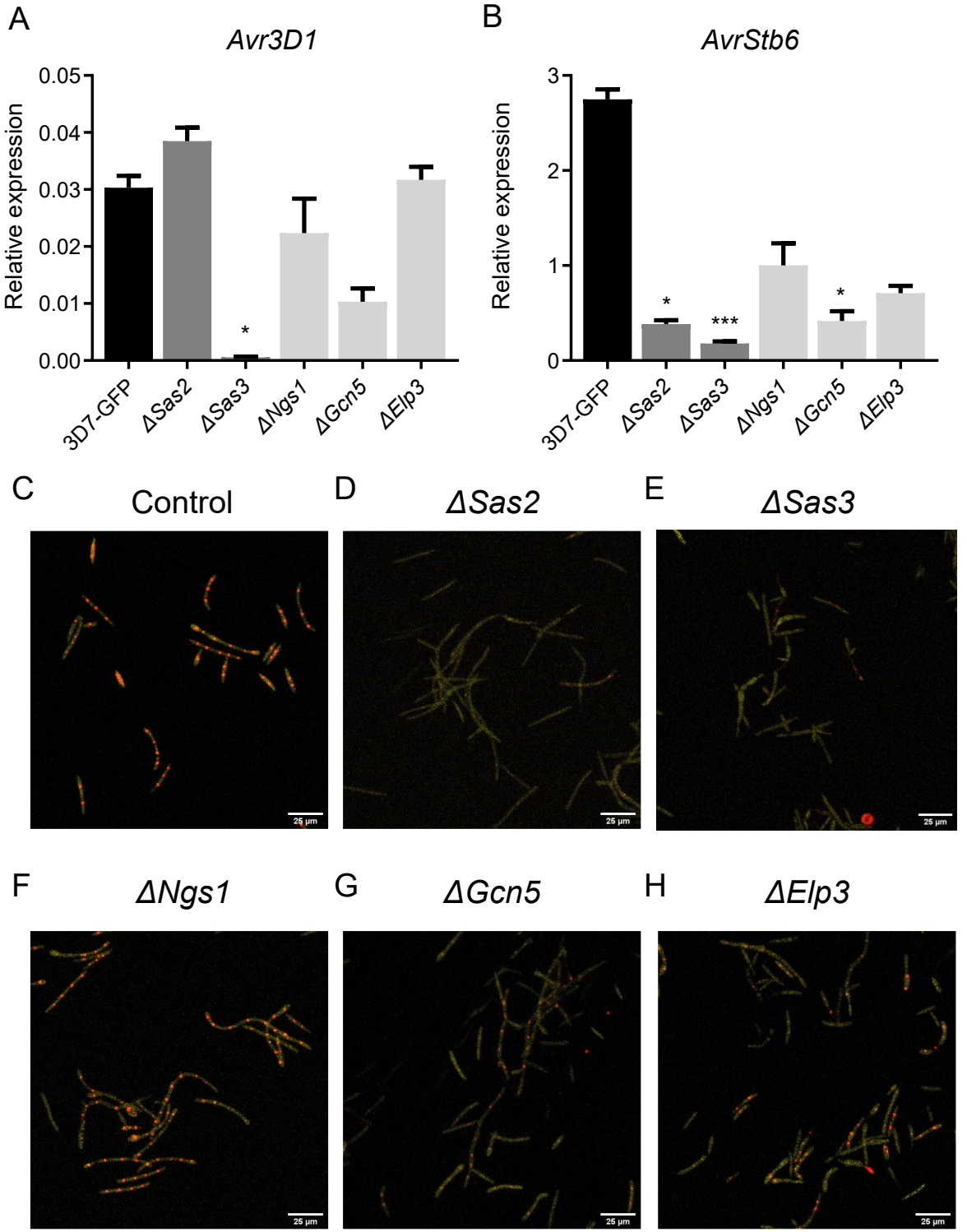
A
Avr3D1
Relative expression
0.05
0.04
0.03
0.02
0.01
0.00
*
3D7-GFP
ΔSas2
ΔSas3
ΔNgs1
ΔGcn5
ΔElp3
B
AvrStb6
Relative expression
3
2
1
0
*
***
*
3D7-GFP
ΔSas2
ΔSas3
ΔNgs1
ΔGcn5
ΔElp3
C
Control
D
ΔSas2
E
ΔSas3
F
ΔNgs1
G
ΔGcn5
H
ΔElp3
25 µm

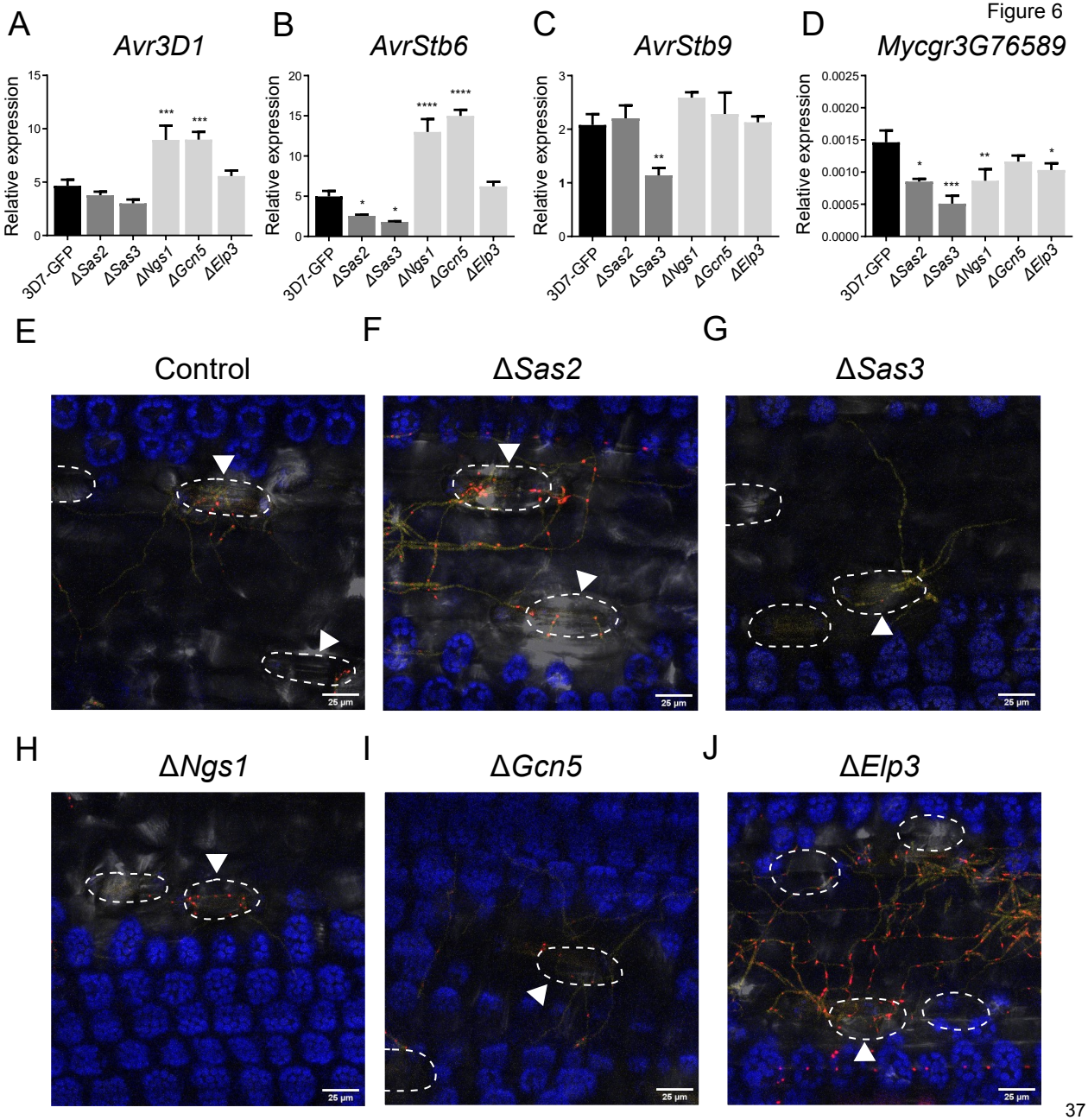
A
Avr3D1
Relative expression
15
10
5
0
***
***
3D7-GFP
ΔSas2
ΔSas3
ΔNgs1
ΔGcn5
ΔElp3
B
AvrStb6
Relative expression
20
15
10
5
0
****
****
*
*
3D7-GFP
ΔSas2
ΔSas3
ΔNgs1
ΔGcn5
ΔElp3
C
AvrStb9
Relative expression
3
2
1
0
**
3D7-GFP
ΔSas2
ΔSas3
ΔNgs1
ΔGcn5
ΔElp3
D
Mycgr3G76589
Relative expression
0.0025
0.0020
0.0015
0.0010
0.0005
0.0000
*
***
**
*
3D7-GFP
ΔSas2
ΔSas3
ΔNgs1
ΔGcn5
ΔElp3
E
Control
F
ΔSas2
G
ΔSas3
25 µm
25 µm
25 µm
H
ΔNgs1
I
ΔGcn5
J
ΔElp3
25 µm
25 µm
25 µm

A

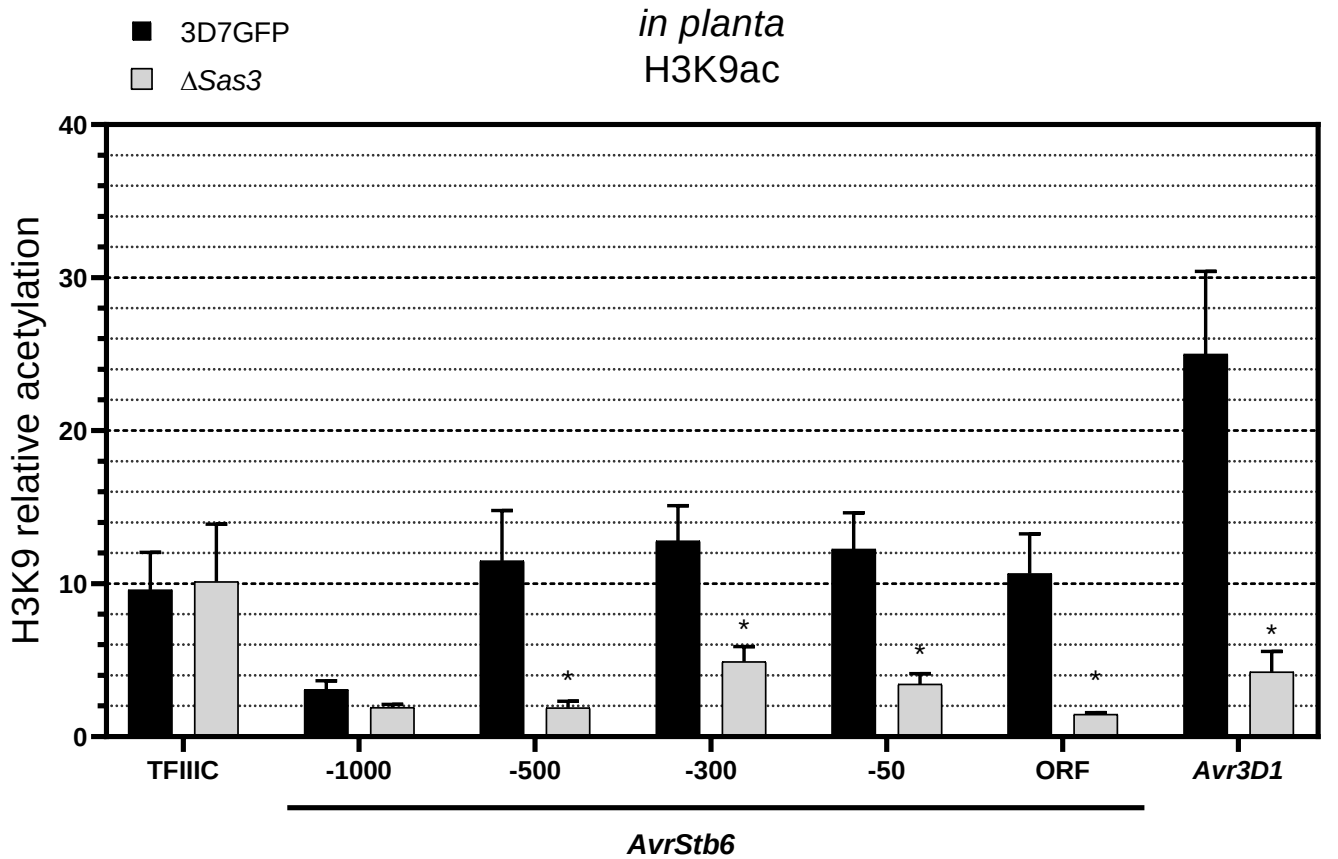
3D7GFP
ΔSas3
in planta
H3K9ac
H3K9 relative acetylation
40
30
20
10
0
TFIIIC
-1000
-500
-300
-50
ORF
Avr3D1
AvrStb6

B

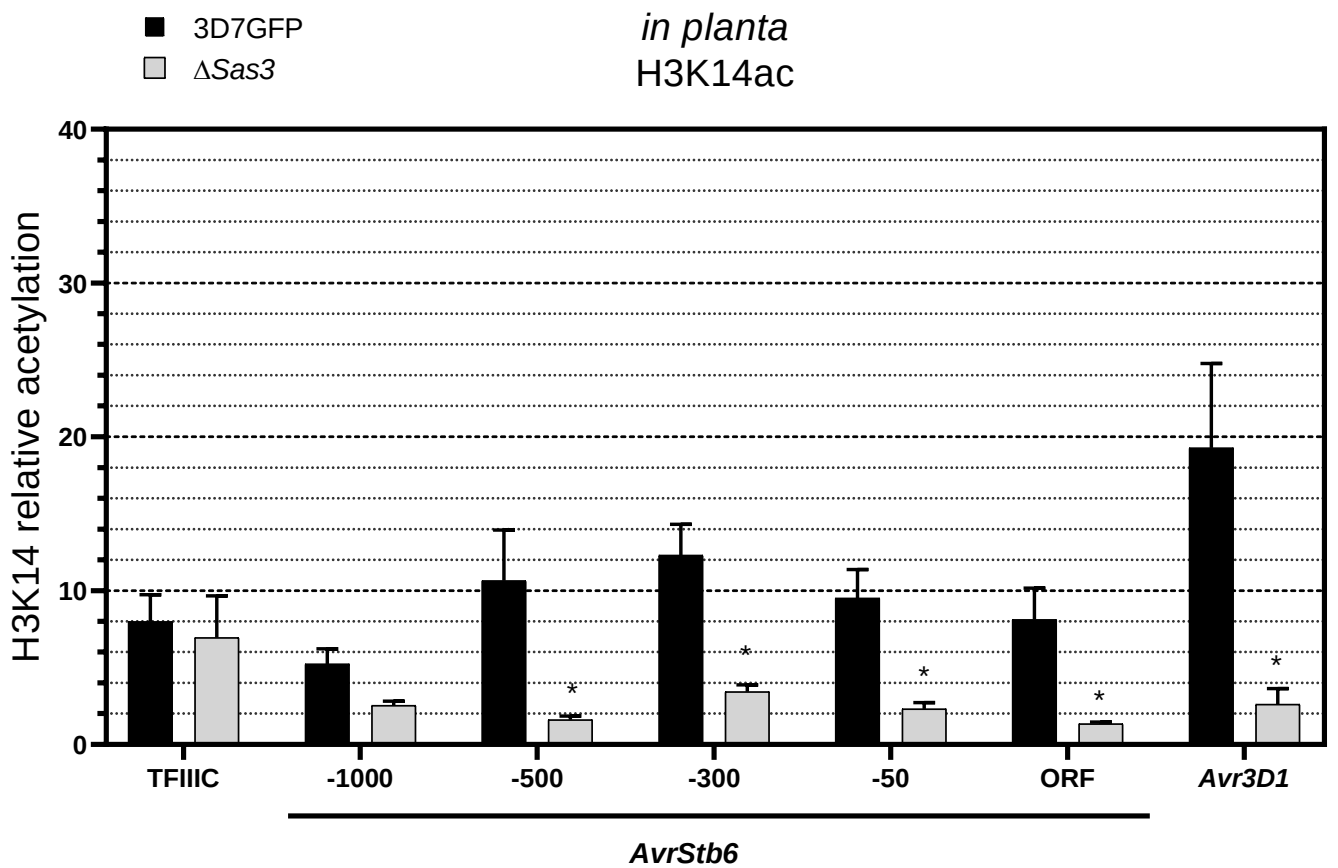
3D7GFP
ΔSas3
in planta
H3K14ac
H3K14 relative acetylation
40
30
20
10
0
TFIIIC
-1000
-500
-300
-50
ORF
Avr3D1
AvrStb6

Figure S1

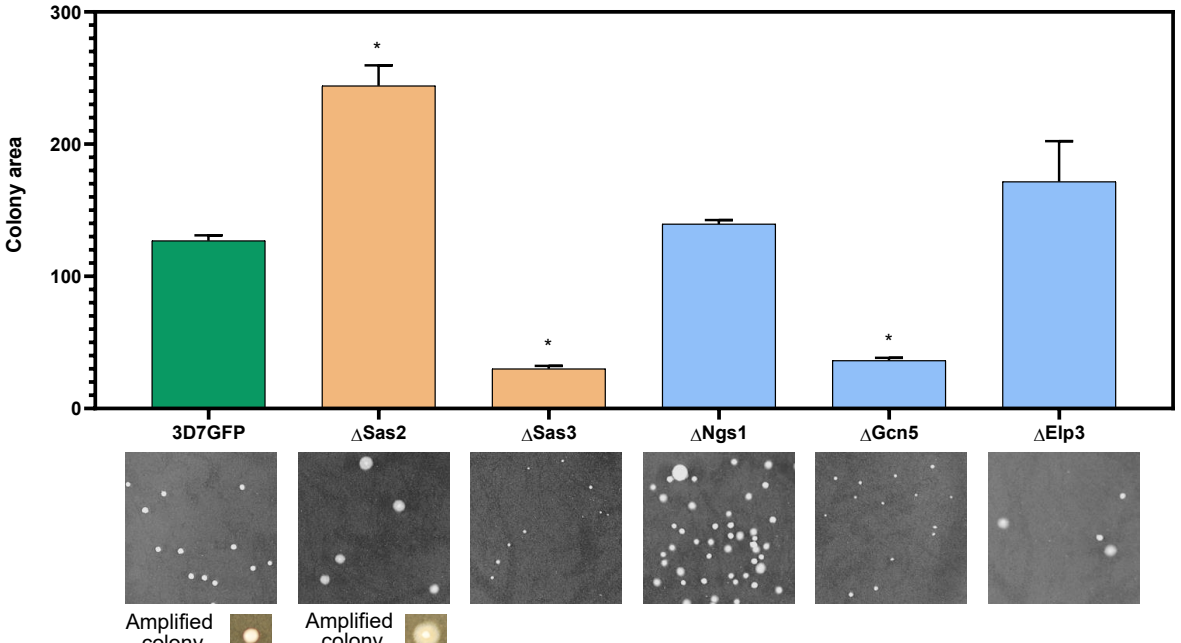
Colony area
300
200
100
0
*
*
*
3D7GFP
ΔSas2
ΔSas3
ΔNgs1
ΔGcn5
ΔElp3
Amplified colony
Amplified colony

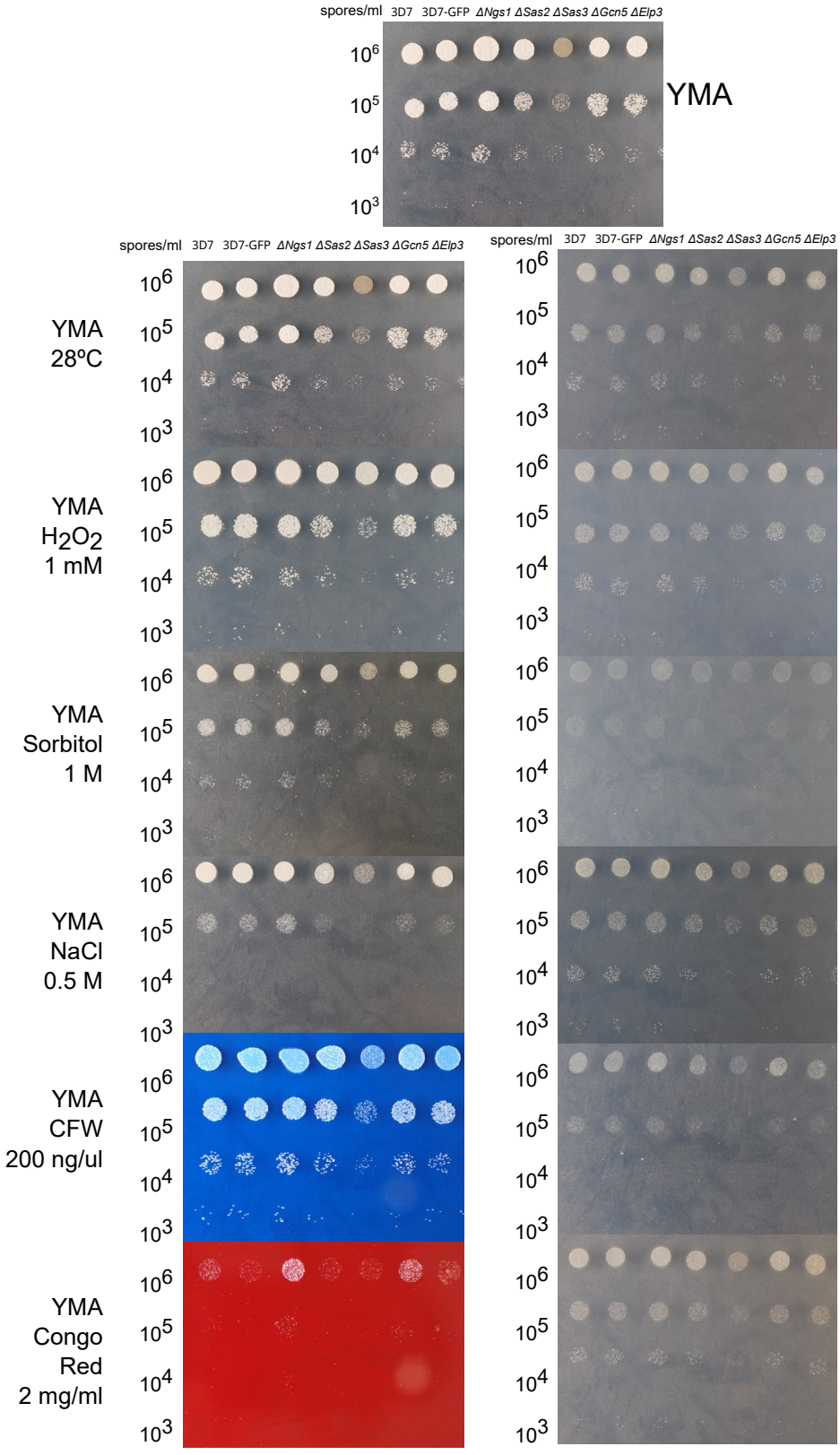
spores/ml
3D7
3D7-GFP
ΔNgs1
ΔSas2
ΔSas3
ΔGcn5
ΔElp3
10^6
10^5
10^4
10^3
YMA
YMA 28ºC
YMA H2O2 1 mM
YMA Sorbitol 1 M
YMA NaCl 0.5 M
YMA CFW 200 ng/ul
YMA Congo Red 2 mg/ml
MM no sucrose
MM Sucrose 1 g/L
MM GlcNAc 2.5 mM
MM Glucose 2.5 mM
MM Galactose 50 mM
MM Fructose 5 g/L

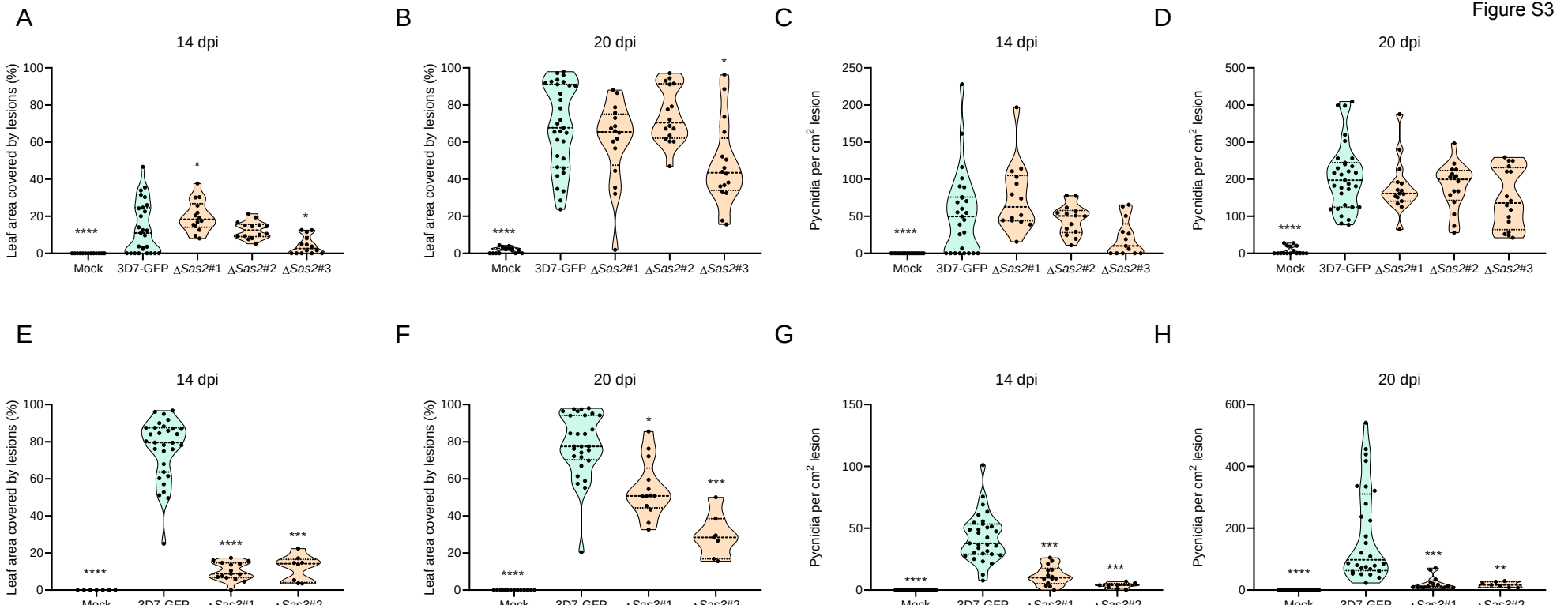
A
14 dpi
Leaf area covered by lesions (%)
Mock
3D7-GFP
ΔSas2#1
ΔSas2#2
ΔSas2#3
B
20 dpi
C
14 dpi
Pycnidia per cm2 lesion
D
20 dpi
E
14 dpi
ΔSas3#1
ΔSas3#2
F
20 dpi
G
14 dpi
H
20 dpi

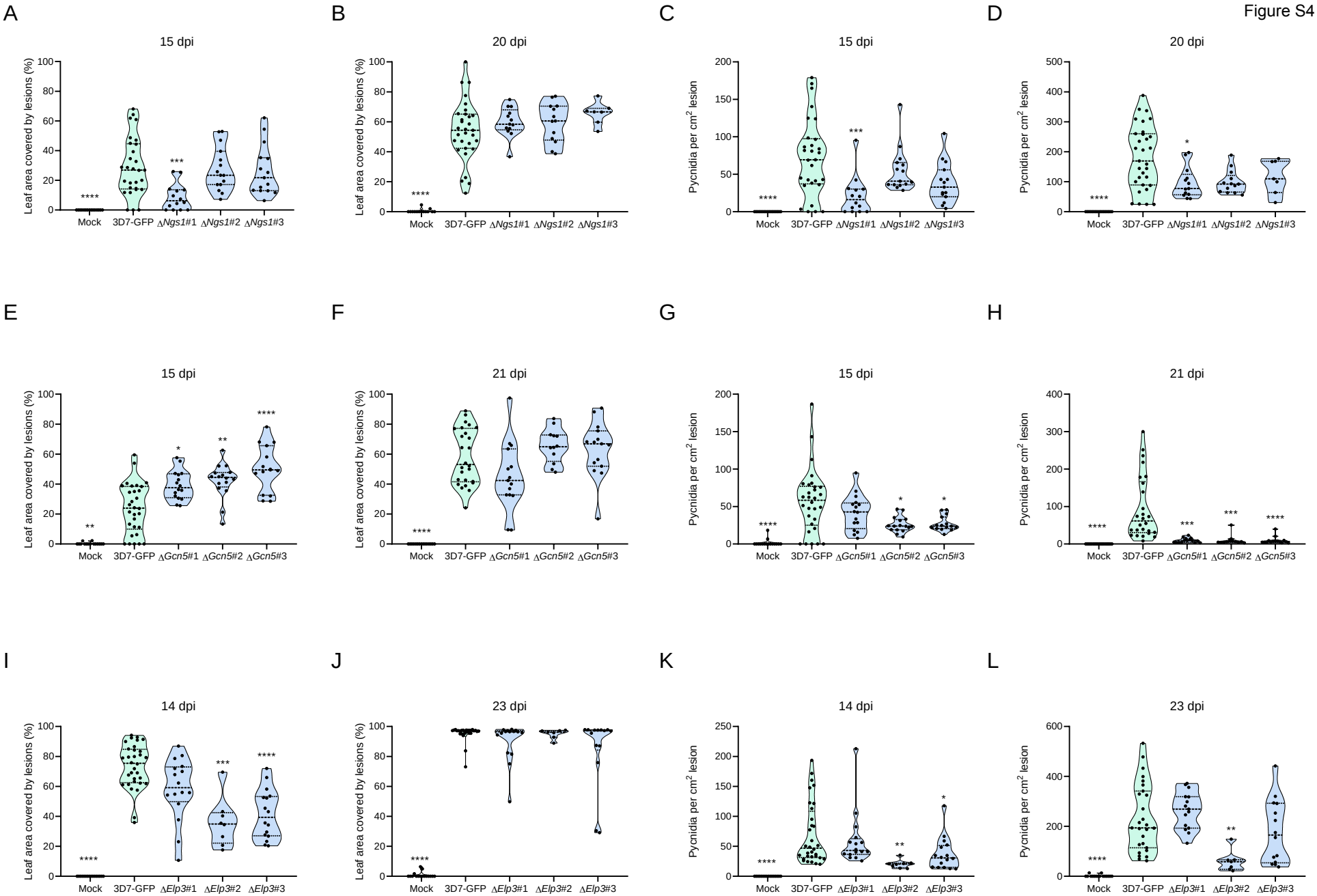
A
15 dpi
Leaf area covered by lesions (%)
Mock
3D7-GFP
ΔNgs1#1
ΔNgs1#2
ΔNgs1#3
B
20 dpi
Leaf area covered by lesions (%)
C
15 dpi
Pycnidia per cm2 lesion
D
20 dpi
Pycnidia per cm2 lesion
E
15 dpi
Leaf area covered by lesions (%)
ΔGcn5#1
ΔGcn5#2
ΔGcn5#3
F
21 dpi
Leaf area covered by lesions (%)
G
15 dpi
Pycnidia per cm2 lesion
H
21 dpi
Pycnidia per cm2 lesion
I
14 dpi
Leaf area covered by lesions (%)
ΔElp3#1
ΔElp3#2
ΔElp3#3
J
23 dpi
Leaf area covered by lesions (%)
K
14 dpi
Pycnidia per cm2 lesion
L
23 dpi
Pycnidia per cm2 lesion

Figure S5

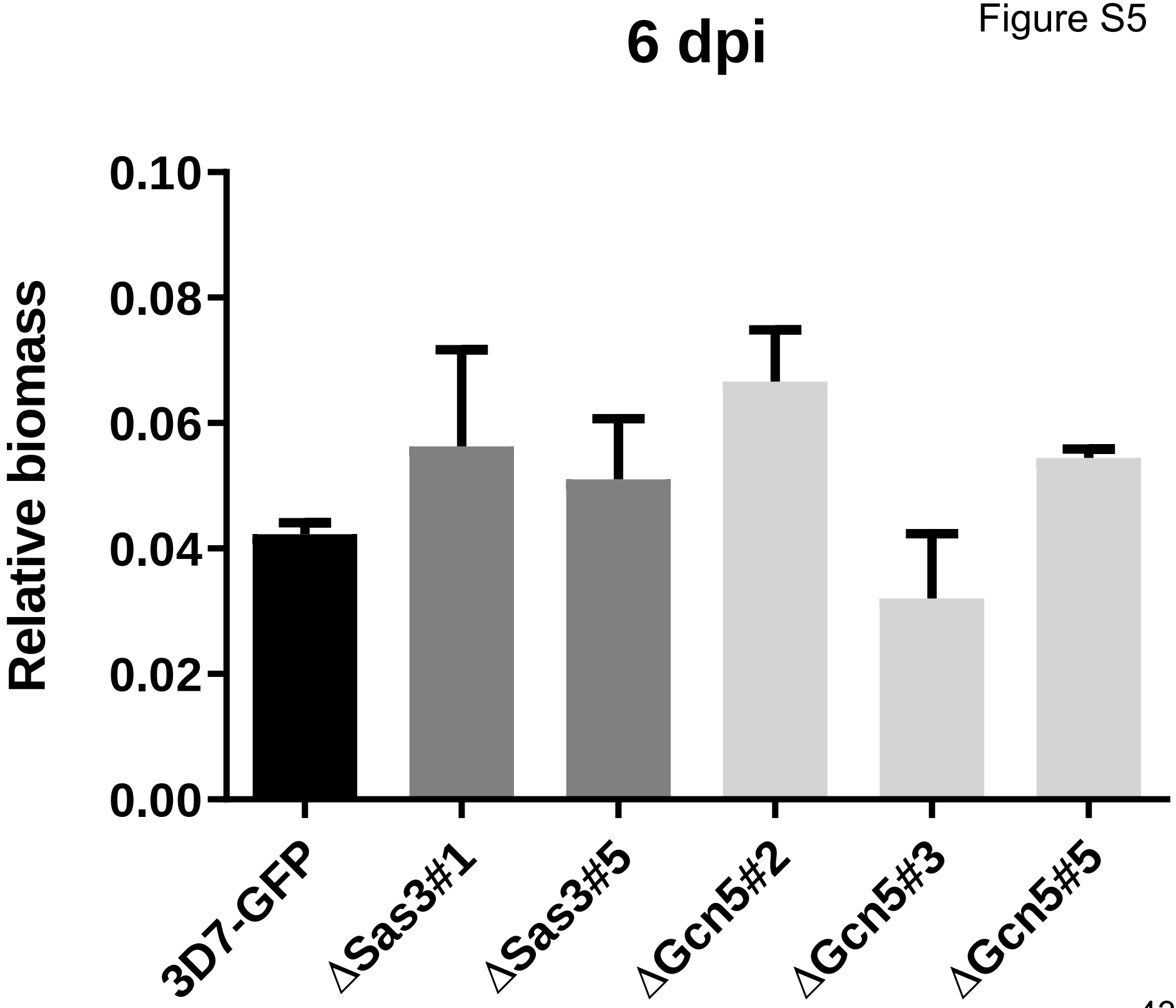
6 dpi
Relative biomass
0.10
0.08
0.06
0.04
0.02
0.00
3D7-GFP
ΔSas3#1
ΔSas3#5
ΔGcn5#2
ΔGcn5#3
ΔGcn5#5


A 3D7-GFP
B ΔSas2
C ΔSas3
D ΔGcn5

A

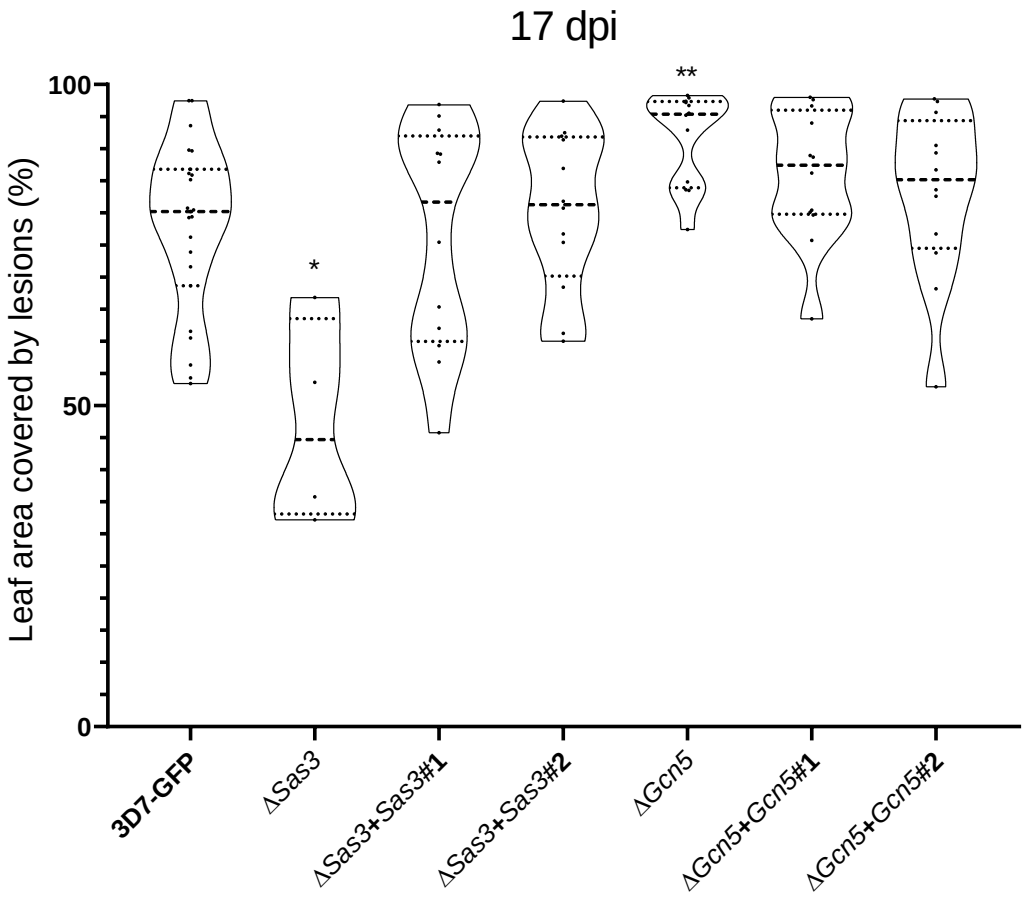
17 dpi
Leaf area covered by lesions (%)
100
50
0
*
**
3D7-GFP
ΔSas3
ΔSas3+Sas3#1
ΔSas3+Sas3#2
ΔGcn5
ΔGcn5+Gcn5#1
ΔGcn5+Gcn5#2

B

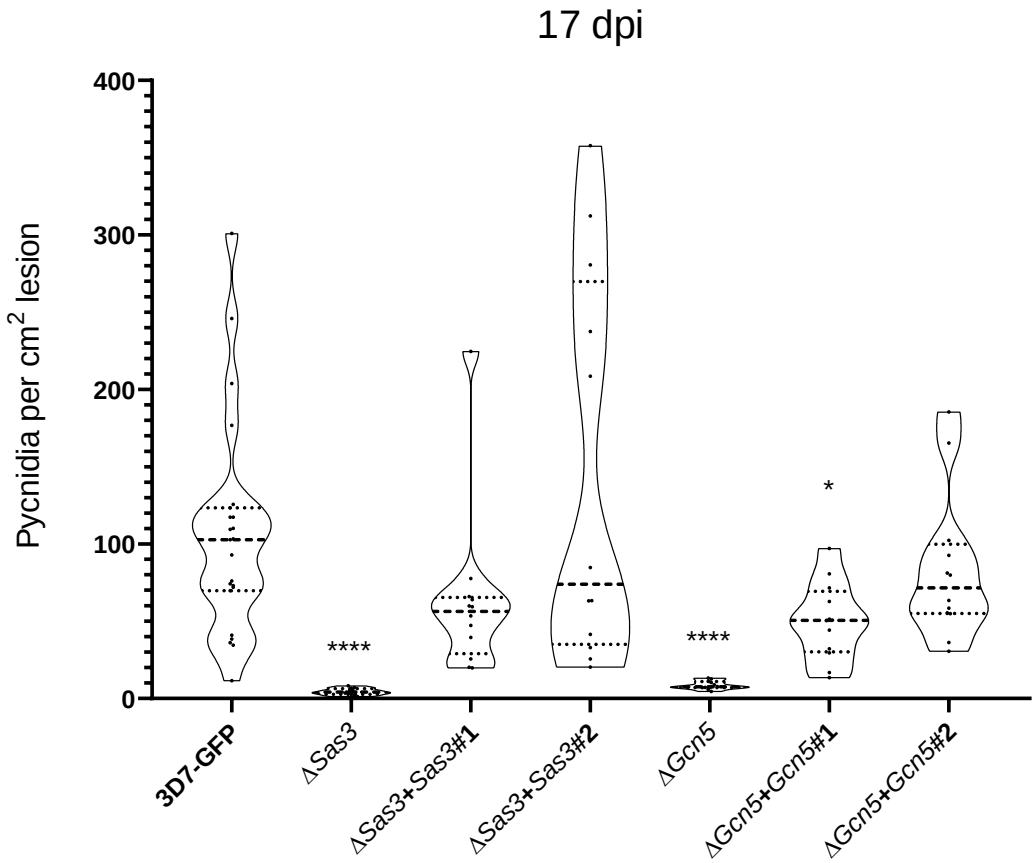
17 dpi
Pycnidia per cm2 lesion
400
300
200
100
0
****
****
*
3D7-GFP
ΔSas3
ΔSas3+Sas3#1
ΔSas3+Sas3#2
ΔGcn5
ΔGcn5+Gcn5#1
ΔGcn5+Gcn5#2

Figure S8

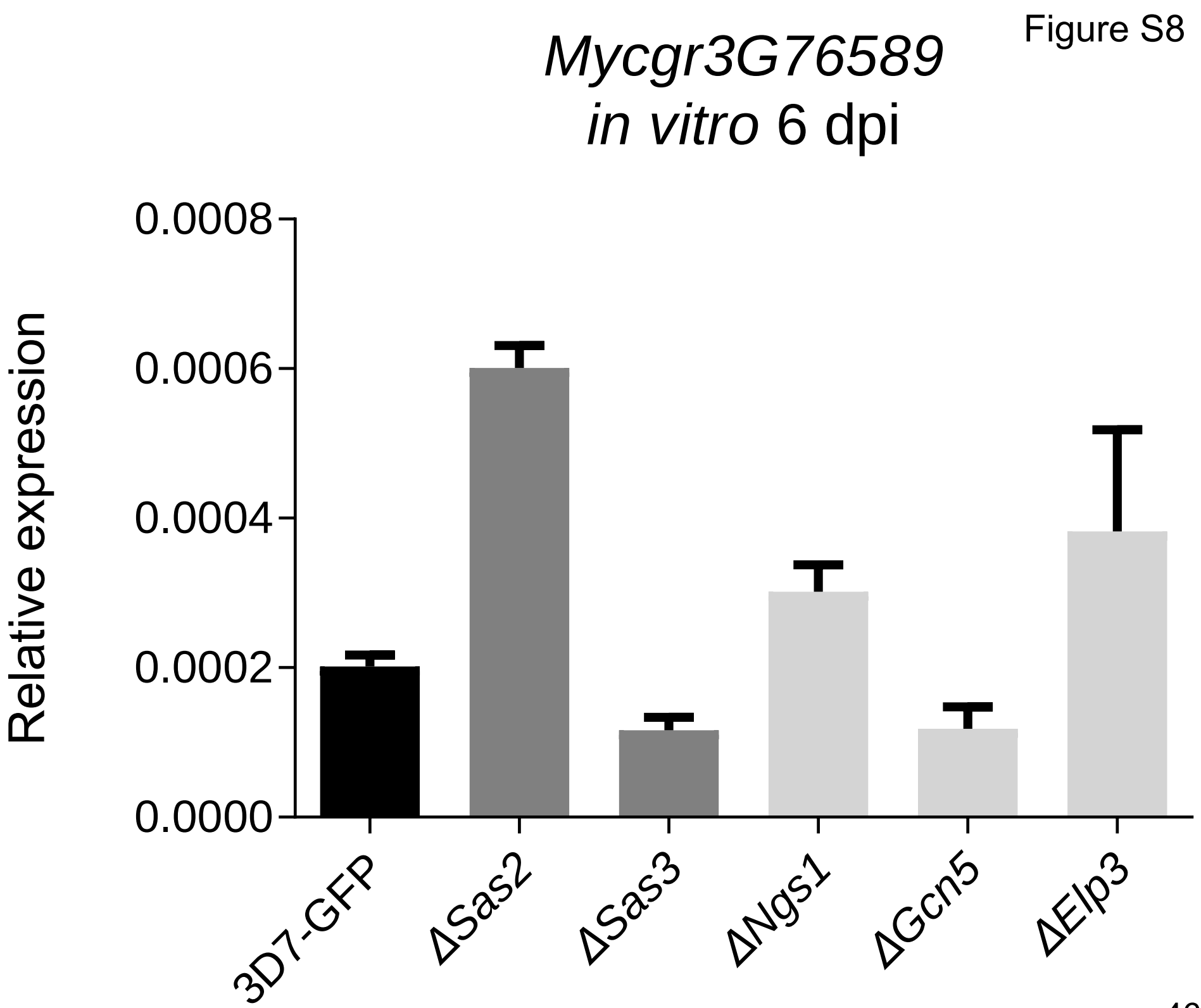
Mycgr3G76589
in vitro 6 dpi
Relative expression
0.0008
0.0006
0.0004
0.0002
0.0000
3D7-GFP
ΔSas2
ΔSas3
ΔNgs1
ΔGcn5
ΔElp3

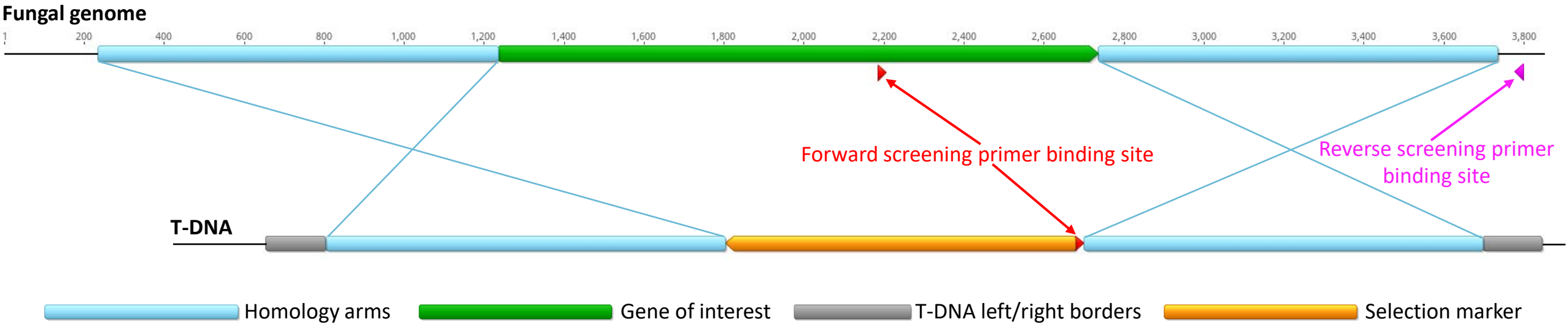
Fungal genome
1
200
400
600
800
1,000
1,200
1,400
1,600
1,800
2,000
2,200
2,400
2,600
2,800
3,000
3,200
3,400
3,600
3,800
Forward screening primer binding site
Reverse screening primer binding site
T-DNA
Homology arms
Gene of interest
T-DNA left/right borders
Selection marker

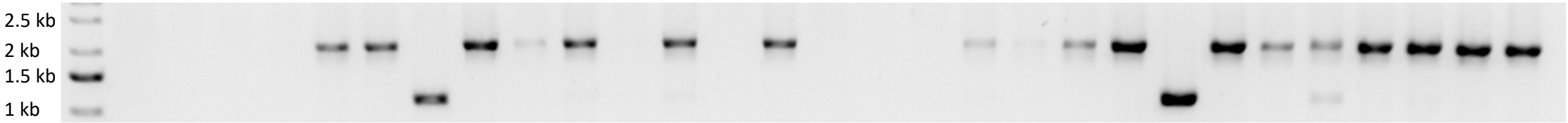
2.5 kb
2 kb
1.5 kb
1 kb